

Submitted to Astrophysical Journal

Galaxy Clusters in the Swift/BAT era: Hard X-rays in the ICM

M. Ajello¹, P. Rebusco², N. Cappelluti^{1,3}, O. Reimer⁴, H. Bohringer¹, J. Greiner¹, N. Gehrels⁵, J. Tueller⁵ and A. Moretti⁶

majello@mpe.mpg.de

A B S T R A C T

We report about the detection of 10 clusters of galaxies in the ongoing Swift/BAT all-sky survey. This sample, which comprises mostly merging clusters, was serendipitously detected in the 15–55 keV band. We use the BAT sample to investigate the presence of excess hard X-rays above the thermal emission. The BAT clusters do not show significant (e.g. $\sim 2\sigma$) non-thermal hard X-ray emission. The only exception is represented by Perseus whose high-energy emission is likely due to NGC 1275. Using XMM-Newton, Swift/XRT, Chandra and BAT data, we are able to produce upper limits on the Inverse Compton (IC) emission mechanism which are in disagreement with most of the previously claimed hard X-ray excesses. The coupling of the X-ray upper limits on the IC mechanism to radio data shows that in some clusters the magnetic field might be larger than 0.5 G . We also derive the first $\log N - \log S$ and luminosity function distribution of galaxy clusters above 15 keV.

Subject headings: galaxies: clusters: general { acceleration of particles { radiation mechanism s: non-thermal { magnetic fields { X-rays: general

¹Max Planck Institut für Extraterrestrische Physik, P.O. Box 1603, 85740, Garching, Germany

²Kavli Institute for Astrophysics and Space Research, MIT, Cambridge, MA 02139, USA

³University of Maryland, Baltimore County, 1000 Hilltop Circle, Baltimore, MD 21250

⁴W. Hansen Experimental Physics Laboratory & Kavli Institute for Particle Astrophysics and Cosmology, Stanford University, USA

⁵Astrophysics Science Division, Mail Code 661, NASA Goddard Space Flight Center, Greenbelt, MD 20771, USA

⁶INAF-OAB, via E. Bianchi 46, Merate (LC) 23807, Italy

1. Introduction

Galaxy clusters are potentially powerful observational probes of dark matter and dark energy. However, the use of clusters to measure cosmological parameters becomes accessible only when astrophysical uncertainties are well understood and controlled. Indeed the non-thermal pressure due to Cosmic Rays (CRs), magnetic fields and turbulence, is a source of systematic bias when cluster masses are estimated using the assumption of hydrostatic equilibrium (e.g. Ensslin et al. 1997). The detection of clusters' X-ray emission above 20 keV is a fundamental step towards the grasp of these processes.

It is well understood that clusters of galaxies contain a large amount of hot gas, called intracluster medium (ICM), that comprises 10–15% of their total mass. Already the first X-ray observations indicated the presence of this optically thin plasma, characterized by an atomic density of about 10^{-4} – 10^{-2} cm⁻³ and temperatures of the order of 10^7 – 10^8 K (e.g. Felten et al. 1966; Catura et al. 1972). Also well established is the fact that the observed X-ray radiation from clusters of galaxies is primarily due to the thermal bremsstrahlung emission of such diffuse hot plasma (Sarazin 1988; Petrosian 2001).

However, evidences gathered at different wavelengths point to the existence of a non-thermal component. In particular the detections of an extended synchrotron radio emission (e.g. Willson 1970; Harris & Miley 1978; Giovannini et al. 1993; Giovannini & Feretti 2000; Kempner & Sarazin 2001; Thierbach et al. 2003) and, more recently, of a possibly non-thermal extreme ultraviolet (EUV) excess (Lieu et al. 1996; Bowyer et al. 1999; Bonamente et al. 2001; Durret et al. 2002) and soft excess (e.g. Werner et al. 2007) suggest the existence of a non-thermal X-ray component originating from a population of relativistic electrons. This scenario is confirmed by the detection of non-thermal emission in the hard X-ray spectra of a few galaxy clusters (see e.g. Kaastra et al. 2008; Rephaeli et al. 2008, for a complete review). Still its actual presence and origin remain controversial (Renaud et al. 2006a; Fusco-Femiano et al. 2007; Werner et al. 2007; Lutovinov et al. 2008).

A non-thermal component could arise from a population of point sources (e.g. AGN as in Katz 1976; Fabian et al. 1976; Fujita et al. 2007) or from inverse Compton (IC) scattering of cosmic microwave background (CMB) photons by relativistic electrons (e.g. Rephaeli 1979; Sarazin 1999). Other possible mechanisms are non-thermal bremsstrahlung (e.g. Sarazin 1999; Sarazin & Kempner 2000) and synchrotron emission from ultra-relativistic electrons (Timokhin et al. 2004; Inoue et al. 2005; Eckert et al. 2007). If the origin of the high-energy emission is IC scattering, then the presence of a large population of relativistic electrons (Lorentz factor $\gg 1000$) is required. This population could have been accelerated in shocks of different origin. Indeed it could be associated to merger shocks (e.g. Fujita et al. 2003; Brunetti et al. 2004), dark matter bow shocks (e.g. Bykov et al. 2000), ram-pressure strip-

ping of infalling galaxies (e.g. de Plaa et al. 2006), jets, Active Galactic Nuclei outbursts (Fujita et al. 2007, in the case of radio mini-halos such as in Perseus cluster), accretion shocks (e.g. Inoue et al. 2005). Non-thermal electrons lose energy on short timescales (below 1 Gyr). Therefore some models consider a continued supply of primary accelerated electrons (i.e. via first order Fermi mechanism), while others assume a constant in-situ re-acceleration via CR collisions or second order Fermi mechanism.

If clusters are a large reservoir of non-thermal particles, then they should emit at higher energies, up to the γ -rays. Indeed, if CRs acceleration is taking place at the shock fronts then γ -rays can be produced via IC, non-thermal bremsstrahlung and π^0 decay (e.g. Rephaeli 1979; Dar & Shaviv 1995; Reimer et al. 2003, 2004; Blasi et al. 2007). A statistical upper limit on the flux above > 100 MeV was obtained by Reimer et al. (2003), analyzing the emission from 58 clusters observed with EGRET.

The role of CRs in the formation and evolution of clusters of galaxies has been much debated. Churazov et al. (2007) suggest that in massive galaxy clusters hydrostatic equilibrium is satisfied reasonably well, as long as the source has not experienced a recent major merger. However, in non-relaxed clusters the non-thermal pressure due to CRs, magnetic fields and micro-turbulence can affect the mass estimates based on hydrostatic equilibrium (e.g. Miralda-Escudé & Babul 1995; Nagai et al. 2007). This would lead to a higher baryonic to total mass ratio. Knowing the importance of CRs, the mechanisms that heat the ICM and the frequency at which it is shocked, is crucial for the upcoming X-ray and Sunyaev-Zeldovich surveys (see Ando & Nagai 2007).

In this paper we report the Swift/BAT all-sky detection of 10 galaxy clusters in the 15–55 keV band. This constitutes the first complete sample so far detected at these energies. We use this sample to investigate the role of non-thermal processes in clusters. The structure of the paper is the following. In §2 we describe the Swift/BAT observations and discuss the properties of each individual cluster (§2.2). In §3.1, we provide, for all the clusters, constraints on the non-thermal emission as well as an estimate of the clusters' magnetic fields (§3.3). The cluster source count distribution and the luminosity function are derived in §4. We discuss the results of our analysis in §5, while §6 summarizes our findings.

We adopt a Hubble constant of $H_0 = 70 h_{70} \text{ km s}^{-1} \text{ Mpc}^{-1}$, $\Omega_M = 0.3$ and $\Omega_b = 0.04$. Unless otherwise stated errors are quoted at the 90% confidence level (CL) for one interesting parameter and solar abundances are determined using the meteoritic values provided in Anders & Grevesse (1989).

2. The BAT X-ray Survey

The Burst Alert Telescope (BAT; Barthelmy et al. 2005), on board the Swift satellite (Gehrels et al. 2004), represents a major improvement in sensitivity for imaging of the hard X-ray sky. BAT is a coded mask telescope with a wide field of view (FOV, $120^\circ \times 90^\circ$ partially coded) aperture sensitive in the 15–200 keV domain. BAT's main purpose is to locate Gamma-Ray Bursts (GRBs). While chasing new GRBs, BAT surveys the hard X-ray sky with an unprecedented sensitivity. Thanks to its wide FOV and its pointing strategy, BAT monitors continuously up to 80% of the sky every day. Results of the BAT survey (Markwardt et al. 2005; Ajello et al. 2008a) show that BAT reaches a sensitivity of 1 mCrab in 1 Ms of exposure. Given its sensitivity and the large exposure already accumulated in the whole sky, BAT poses itself as an excellent instrument for looking for the (faint) emission of galaxy clusters above 15 keV.

For the analysis presented here, we used all the available data taken from January 2005 to March 2007. Since most of the cluster emission is expected to be thermal and thus rather soft, the survey chosen energy interval is 15–55 keV. The lower limit is dictated by the energy threshold of the detectors. The upper limit was chosen as to avoid the presence of strong background lines which could worsen the overall sensitivity. The data screening was performed according to Ajello et al. (2008a). The all-sky image is obtained as the weighted average of all the shorter observations. The average exposure time in our image is 3 Ms, being 1.3 Ms and 5 Ms the minimum and maximum exposure times respectively. The final image shows a Gaussian normal noise. Source candidates were identified as excesses above the 5σ level. All these objects are then fitted with the BAT point spread function (using the standard BAT tool `batcelldetect`) to derive the best source position.

As shown in Ajello et al. (2008a) cross-correlating the BAT sources with the ROSAT All-Sky Survey Bright Source Catalogue (Voges et al. 1999) provides an easy and solid way to identify a large fraction ($\sim 70\%$) of them. Most of the uncorrelated sources are not present in the ROSAT survey because of absorption (either along the line of sight or intrinsic to the source). The unidentified sources are targeted by Swift/XRT which in less than 10 ks can pinpoint the exact counterpart (e.g. Tueller et al. 2005a,b; Kennea et al. 2005).

The details about the complete source list will be given in an upcoming publication. Here we report about the detection of galaxy clusters above 5σ in the 15–55 keV band.

2.1. Clusters Identification

Identifying clusters of galaxies as counterpart of BAT objects is not a straightforward process. Indeed, coded mask telescopes are rather insensitive to diffuse sources which extend over angles much larger than the projection of the mask tile on the sky (i.e. a few tens of arcmin for BAT). Even though procedures exist to quantify the extent of diffuse sources in coded mask instruments (see Renaud et al. 2006a,b; Lutovinov et al. 2008, for the case of the Coma Cluster), their application is limited only to high signal-to-noise (S/N) objects. Given the extent of the BAT PSF (22°), Coma is the only object whose emission is clearly extended in our investigation. Thus, for all other objects, the morphology of the source cannot be used to understand whether the BAT source is associated to the cluster or only to its brightest AGN. We therefore performed a spectral analysis (see § 2.2) of those BAT sources that are spatially associated with galaxy clusters. All sources presented here show a significant thermal component that we interpret as thermal bremsstrahlung from the ICM and thus are securely associated with the proposed clusters. Our sample contains 10 galaxy clusters. Table 1 reports the position, significance, total exposure time and other details of all the detected clusters.

2.2. Spectral Analysis

For each galaxy cluster we extracted a 15{195 keV spectrum with the method described in Ajello et al. (2008c). Here we recall the main steps: the details can be found in the aforementioned paper. For a given source, we extract a spectrum from each observation where the source is in the field of view. These spectra are corrected for residual background contamination and for vignetting; the per-pointing spectra are then (weighted) averaged to produce the final source spectrum. Thus, the final spectrum represents the average source emission over the time-span considered here (2.5 years). The accuracy of these spectra is discussed in § 2.3.

For all the clusters, we extracted a 0.3{10 keV spectrum using archival observations of XMM-Newton, Chandra, and Swift/XRT. Considering that for BAT all clusters, except Coma, are point-like objects we extracted (unless otherwise stated) all cluster photons within 10° from the position of the BAT centroid. In most cases, this selection allows us to include most of the emission of the cluster. For those cases where there is clearly emission outside of our selection region¹, we accounted for the missed flux using the beta profiles available

¹ In some cases the extent of the selection region is limited by the size of the CCD.

in literature. The details are given in the case-by-case section (x 2.4). The level of the background was evaluated in regions of the CCDs not contaminated by the cluster emission or using blank-sky observations (e.g. Lumb et al. 2002; Read & Ponman 2003). In all cases, we considered the systematic uncertainty connected to the background subtraction, in the 0.3–10 keV band, to be 2%. All spectra were rebinned in order to have a minimum of 50 counts (7) per bin.

As a standard procedure, we started fitting all the spectra with the most simple and plausible spectral model. In all cases this was a single-temperature thermal model with absorption fixed at the Galactic value. Only if the value of the χ^2/dof was greater than 1, we tried to add a second thermal model or a power law. In this case we chose the model which produced the best improvement in the χ^2 (evaluated using the F-test) and the best residuals.

Various authors have reported detections of hard X-ray excesses for some of the clusters present in our sample. For those cases where we do not detect directly such component, we tested whether our data are consistent with the reported non-thermal hard X-ray emission. This was done adding a power law to the thermal model used. We fixed the power-law index to 2.0, which is a value generally accepted for the non-thermal hard X-ray component generated by IC of relativistic electrons on CMB photons (e.g. Reimer et al. 2004; Nevalainen et al. 2004). We then let the power-law normalization vary until the χ^2 increment was larger than 2.7 (6.64). According to Avni (1976), this gives the 90% (99%) confidence level on the parameter of interest. This allows us to investigate the level of non-thermal flux which is consistent with our data.

2.3. Accuracy of BAT spectra

When dealing with spectral features which are at the limiting sensitivity of a given instrument, it is important to make sure that all systematic uncertainties have been carefully taken care of. In order to test the reliability of our spectral extraction method, we extracted > 160 spectra at random positions in the sky at least 30° away from the potential (or detected) X-ray sources reported in the INTEGRAL reference catalog (Ebisawa et al. 2003). The mean (raw) exposure of our spectral sample is 4.6 Ms. In each energy channel, the average flux is consistent within 1 with zero as expected for pure noise and for efficient background subtraction. Moreover, the S/N distributions (i.e. flux divided by its error in a given energy channel; examples are shown in Fig. 1) are all consistent with Normal Gaussian distributions. Both findings show that our spectra are trustworthy in the whole energy range (15–200 keV) and that uncertainties are well estimated.

Moreover, we can use the randomly extracted spectra to measure the average spectral sensitivity of BAT in a given energy channel. This is done deriving for each energy channel the standard deviation of the flux distribution. As shown in Fig. 2, the 3 σ sensitivity in each energy channel is very close, except above 100 keV, to 1 mCrab.

2.4. Individual Cluster Analysis

2.4.1. Perseus

Swift J0319.8+4130 is certainly associated with the Perseus cluster (Abell 426). The BAT detection (see Fig. 3) is well centered on the cluster. Perseus is one of the most studied galaxy clusters and its detection in X-rays dates back to the seventies (Fritz et al. 1971; Forman et al. 1972). XMM-Newton observations (Churazov et al. 2003) showed that the central region is contaminated by the emission of the AGN hosted by the brightest galaxy in Perseus, NGC 1275. A hard X-ray component has been detected with HEAO 1 by Primini et al. (1981). Nevalainen et al. (2004) used BeppoSAX and previous RXTE measurements to prove that this non-thermal component is variable and must therefore be connected to the central bright AGN. Sanders & Fabian (2007) reported, using Chandra, the presence of non-thermal X-ray emission in the core of Perseus in correspondence of the radio minihalo (i.e. Gisler & Miley 1979; Gitti et al. 2002). This non-thermal emission, which displays a power-law behavior with photon index of 2.0, seems to exceed the flux of NGC 1275 by a factor ~ 3 (Sanders et al. 2004).

The BAT spectrum shows evidences of an hard X-ray excess. Indeed, it can be fit by a steep power-law (photon index of 3.5 ± 0.1 and $\chi^2_{\text{red}} = 2.3$) while it rejects a simple bremsstrahlung fit ($\chi^2_{\text{red}} = 3.6$). The fit improves ($\chi^2_{\text{red}} = 1.50$) if we use a composite model, sum of the (bremsstrahlung like) gas emission and the (power-law like) AGN emission. The improvement of the fit is statistically significant as confirmed by the f-test probability of $1.2 \cdot 10^{-2}$. The best fit temperature is $6.4^{+2.3}_{-2.3}$ keV and the photon index is $2.5^{+1.9}_{-1.0}$. If we fix the photon index at the value (1.65) determined by Churazov et al. (2003), we derive an extrapolated 0.5–8.0 keV luminosity of $0.4 \cdot 10^{42}$ erg s $^{-1}$ which is in agreement with the luminosity measured by XMM-Newton. This supports the idea that the hard-tail seen in the BAT spectrum is due to NGC 1275 and not to a non-thermal component originated in the ICM. Moreover, if we extrapolate, using a power-law with photon index of 2.0, the non-thermal flux found in the 2–10 keV range by Sanders et al. (2005) to the 50–100 keV band we get a value of $2.7 \cdot 10^{11}$ erg cm $^{-2}$ s $^{-1}$. This flux is a factor ~ 4 larger than the total cluster flux observed by BAT in the same energy band. Recently Molendi & Gastaldello (2008) analyzed a long XMM-Newton observation and did not find evidence for non-thermal

emission. According to them the discrepancy between the Chandra and XMM-Newton results is due to a problem in the effective area calibration of Chandra.

An XRT observation of 5.4 ks was carried out in July 2007. Given the size of the XRT CCD, we extracted all source photons within $6''$ from the BAT centroid. The surface brightness profile of Perseus is best described by the sum of a power-law and of a beta model. Adopting this model, as suggested by Ettori et al. (1998), yields that 94% of the total cluster emission falls within our selection. The joint XRT+BAT spectrum can be fitted by a sum of two APEC (Smith et al. 2001) models and a power law. The low-temperature component, which accounts for the cool core of the cluster, has a temperature of $3.0^{+0.4}_{-0.7}$ keV and an abundance of $0.43^{+0.20}_{-0.16}$ solar. The warmer component displays a temperature of $6.40^{+0.62}_{-0.71}$ keV and an abundance of $0.31^{+0.15}_{-0.15}$ solar. These results are in line with the analyses of Churazov et al. (2003) and Sanders et al. (2005). Both the power-law photon index of $1.7^{+0.3}_{-0.7}$ and the luminosity in the 0.5–8.0 keV band of 8×10^{42} erg s⁻¹ are compatible with the values found, for NGC 1275, by Churazov et al. (2003) and the ones determined in the next section. The photon index is slightly harder than the average photon index (2.0) of BAT AGN, however it is not unusual for radio-loud objects (e.g. Ajello et al. 2008c).

The Nucleus of Perseus

In order to study more in details the nuclear emission, we analyzed a 125 ks long XMM-Newton observation (observation 0305780101). We extracted the spectrum of the nucleus in a radius of $25''$ and evaluated the local background in an annulus around the source region. We note that the results presented here are not sensitive to the radius of the extraction region if this is in the $10''$ – $30''$ range. The 0.2–9.0 keV spectrum of the nucleus is well fitted ($\chi^2/\text{dof} = 960.1/731$) by an absorbed power-law model with absorption consistent with the Galactic one and a photon index of 1.60 ± 0.02 . Moreover, we find evidence (at the 95% CL) of a K α Iron line with equivalent width of 90.2 ± 45.0 eV. An absorbed APEC model with a temperature of 12.6 ± 0.7 keV provides a worst fit ($\chi^2/\text{dof} = 1167.1/732$) to the data. In particular, the absorption would be required to be lower than the Galactic one at 99% CL. This fact, in conjunction with the presence of the Iron line, supports the evidence that the non-thermal emission in the nucleus of the Perseus cluster is produced by the central AGN. The non-thermal luminosities in the 0.5–8.0 keV and 2.0–10.0 keV bands are $7.6^{+0.2}_{-0.2} \times 10^{42}$ erg s⁻¹ and $6.5^{+0.2}_{-0.2} \times 10^{42}$ erg s⁻¹ respectively. In order to check these results we extracted a similar spectrum of the nucleus using Swift/XRT data and selecting an extraction region of $10''$. The XRT data are compatible with the XMM-Newton one. Indeed, fixing the absorption at the Galactic value we find that the XRT data are compatible with a power-law model with a photon index of 1.6 ± 0.1 and that the 2.0–10.0 keV luminosity is

$8.2^{+1.1}_{-1.0} \times 10^{42} \text{ erg s}^{-1}$. Thus, the nucleus displays a moderate variability between the XMM-Newton and Swift/XRT observation epochs. This supports, once more, the interpretation that the non-thermal emission is produced by the central AGN.

2.4.2. Abell 3266

Swift J0431.3-6126 is associated with Abell 3266. Figure 4 shows that the BAT source is well centered on the cluster emission as seen by ROSAT. A 3266 (also known as Sersic 40-6) was first detected in X-rays by the UHURU satellite (Giacconi et al. 1972). Accordingly to many authors (e.g. Sauvageot et al. 2005; Finoguenov et al. 2006, and references therein) Abell 3266 recently underwent a major merger, probably with a subcluster that was stripped during the encounter with A 3266 dense core. De Grandi & Molendi (1999) and Nevalainen et al. (2004) observed Abell 3266 with BeppoSAX. The first group modeled the BeppoSAX broad-band spectrum ($2\text{--}50 \text{ keV}$) with a simple optically thin thermal emission model at the temperature of $8.1 \pm 0.2 \text{ keV}$, while the second group found a marginal evidence (0.8 σ) of non-thermal X-ray excess.

The BAT spectrum, shown in Fig. 4, is consistent with the findings of De Grandi & Molendi (1999). A bremsstrahlung model with a plasma temperature of $6.9^{+2.5}_{-1.8} \text{ keV}$ provides indeed a good fit to the data ($\chi^2/\text{dof} = 7.2/10$). XMM-Newton observed Abell 3266 for 8.6 ks in September, 2000. The cluster is not centered on the EPIC-PN CCD. Thus we could extract only photons within a circular region of $8''$ radius centered on the BAT centroid. In order to estimate the flux missed by our selection, we adopt, for the cluster surface brightness, a beta profile with $\beta = 0.51$ and core radius $R_c = 3.1''$ (Sauvageot et al. 2005). According to our estimate 80% of the total cluster flux is contained in our selection. Therefore, when fitting jointly the XMM-Newton and the BAT data, we use such cross-normalization factor. The combined XMM-Newton+BAT spectrum is well fitted by a single APEC model with a plasma temperature of $8.0^{+0.4}_{-0.4} \text{ keV}$ and $0.41^{+0.13}_{-0.13}$ solar abundance. We derive a 99% CL limit on the non-thermal $50\text{--}100 \text{ keV}$ flux of $5.70 \times 10^{13} \text{ erg cm}^{-2} \text{ s}^{-1}$.

Extended radio emission correlated with A 3266 has been reported (Robertson & Roach 1990; Brown & Burns 1991). In order to estimate the magnetic field (see x 3.1, Table 3), we adopt the radio data from Brown & Burns (1991), based on the Parkes catalogue, namely a flux density $S_{2700 \text{ MHz}} = 1.070 \text{ Jy}$ and a spectral index $\alpha = 0.95$.

2.4.3. Abell 0754

Swift J0908.9-0938 is associated with the well studied cluster of galaxies Abell 0754. X-ray maps indicate that A 0754 is far from hydrostatic equilibrium, experiencing a violent merger (i.e. Henry & Briel 1995; Henriksen & Markevitch 1996). Its detection by RXTE (Valinia et al. 1999; Revnivtsev et al. 2004) and BeppoSAX (Fusco-Femiano et al. 2003) above 15 keV make the association of the cluster with the BAT source secure. While the RXTE detections do not measure any significant hard X-ray excess, BeppoSAX detects a hard tail with a significant deviation from the thermal component in the 50-70 keV energy range. It is worth noting that the BAT centroid² falls $\sim 6''$ west of the brightest region of the cluster (see Fig. 5). Chandra analysis of the gas temperature spatial distribution shows indeed that the BAT position corresponds to regions of hot ($T \sim 10-15$ keV) gas (Markevitch et al. 2003). The analysis of XMM-Newton data confirms the existence of hot regions in the west part of the cluster (Henry et al. 2004). On the other hand, centroid shifts as a function of the waveband are a common indication of a merging cluster (O'Hara et al. 2004).

The BAT spectrum, shown in Fig. 5, is well fitted ($\chi^2/\text{dof} = 63/9$) by a single bremsstrahlung model with a plasma temperature of $9.9^{+4.3}_{-2.6}$ keV. This is in good agreement with the temperature of $9.4^{+0.16}_{-0.17}$ keV reported by Fusco-Femiano et al. (2003) and 9.0 ± 0.13 keV reported by Valinia et al. (1999). The BeppoSAX 10-40 keV non-thermal flux of $1.6 \times 10^{12} \text{ erg cm}^{-2} \text{ s}^{-1}$ is consistent with the (90%) upper limit from BAT of $6.5 \times 10^{12} \text{ erg cm}^{-2} \text{ s}^{-1}$.

XMM-Newton observed A 0754 for 11 ks in May, 2001. The XMM-Newton/BAT data are well fitted by a single APEC model with a plasma temperature of $8.5^{+0.19}_{-0.13}$ keV and 0.29 ± 0.03 solar abundance. Adding a power-law model, with photon index fixed to 2.0, improves the fit (F-test probability 4.6×10^{-9}). The best fit temperature is 9.3 ± 0.4 keV and the non-thermal 50-100 keV flux is $7.6^{+2.4}_{-2.7} \times 10^{13} \text{ erg cm}^{-2} \text{ s}^{-1}$. The non-thermal flux in the 10-40 keV band is $1.7^{+0.2}_{-0.6} \times 10^{12} \text{ erg cm}^{-2} \text{ s}^{-1}$ and is in good agreement with the non-thermal flux measured by Fusco-Femiano et al. (2003). However, Fusco-Femiano et al. (2003) also discuss the possibility that the non-thermal flux be produced by the BL Lac object 26W 20. This object lies $24''$ away from the BAT centroid, and outside the XMM-Newton field of view, thus we can rule out that it is contributing to the detected non-thermal flux.

However, we note that several point-like objects appear in the XMM-Newton image

²For an 8 σ detection, the expected maximum offset of the BAT centroid is $2.5''$ (see Fig. 10 in Ajello et al. 2008a).

and within 10^0 from the BAT centroid. A simple hardness ratio analysis reveals that the hardest object is located at R.A., Dec. = 09 09 13.7, -09 43 05.4. The likely counterpart is 2MASX 09091372-0943047 for which beside the magnitude ($m_{\text{mag}} = 20.0$) nothing else is known. The XMM-Newton spectrum is extremely hard. It can be well represented, in the 0.1–10 keV energy range, by an absorbed power-law with photon index of $1.23^{+0.33}_{-0.24}$ and absorption of $5.6^{+5.4}_{-2.6} \times 10^{21} \text{ atom cm}^{-2}$. The source flux extrapolated to the 10–40 keV band is $(1.3 \pm 0.3) \times 10^{12} \text{ erg cm}^{-2} \text{ s}^{-1}$. It is thus clear that this single source accounts for the non-thermal flux detected both by our and Fusco-Femiano et al. (2003) analyses.

Valinia et al. (1999) and Fusco-Femiano et al. (2003) derive a lower limit for the magnetic field of 0.2 G and 0.1 G respectively. Our estimate of B , reported in Table 3, uses the VLA observations from Fusco-Femiano et al. (2003) ($S_{1365 \text{ MHz}} = 86 \text{ mJy}$, $\alpha = 1.5$) and is consistent with the results of Bacchi et al. (2003) and of Fusco-Femiano et al. (2003).

2.4.4. Coma

Swift J1259.4+2757 is associated with the Coma cluster which is one of the best studied cluster of galaxies. Coma (aka A 1656) is a particularly rich and symmetric merging cluster. It has been known as a diffuse X-ray and radio source since forty years (Felten et al. 1966; Forman et al. 1972; Willson 1970). The cluster hosts a powerful radio halo (Ferettil & Giovannini 1998) and both BeppoSAX (Fusco-Femiano et al. 1999) and RXTE (Rephaeli 2001; Rephaeli & Gruber 2002) revealed the existence of non-thermal hard X-ray emission.

However, the detection of this hard X-ray excess is still quite controversial. Indeed, the positive BeppoSAX detections (Fusco-Femiano et al. 1999, 2004) of hard X-ray excess were challenged by Rossetti & Molendi (2004, 2007). According to Rossetti & Molendi (2007), the significance of the non-thermal excess changes (decreases) with the best-fit plasma temperature and only a certain set of assumptions (e.g. temperature of the ICM) leads to a significant hard X-ray excess. However, recently Fusco-Femiano et al. (2007), using different software analyses and studying a large set of background observations, were able to confirm their previous finding. Independently of the BeppoSAX results, the RXTE detection (Rephaeli 2001; Rephaeli & Gruber 2002) of the hard X-ray excess remains unchallenged.

Lately, Coma has also been targeted by INTEGRAL (Eckert et al. 2007; Lutovinov et al. 2008). Eckert et al. (2007) show, in their combined XMM-Newton+INTEGRAL analysis, the presence of a hotter region (gas temperature of 12–2 keV as compared to 7.9–0.1 keV of the center) in the south-west region. The authors favor the possibility that this emission is produced by IC scattering because its spatial distribution overlaps the halo of radio syn-

chrotron radiation. Lutovinov et al. (2008) using INTEGRAL, ROSAT and RXTE data showed that the global Coma spectrum is well approximated by a thermal emission model only and found very marginal evidences (1.6σ) for hard X-ray excess. Thus, in light of these results the evidences for non-thermal emissions in Coma seem not conclusive.

Coma is the only cluster in our sample whose extent is larger than the BAT PSF. The analysis of point-like sources in the vicinity of the Coma cluster shows that the PSF full width at half maximum (FWHM) is $22''$ while the FWHM of the Coma detection is $26''$. Using a simple Gaussian profile for the surface brightness of Coma yields a $1''$ extent in the $10''\{15''$ range. This is in agreement with the morphological analysis of Eckert et al. (2007). Moreover, from Figure 6, the offset between the BAT and the ROSAT centroids is apparent. Indeed, the BAT centroid falls $4''$ west of the ROSAT surface brightness peak. As discussed by Eckert et al. (2007) and Lutovinov et al. (2008) for INTEGRAL, the high-energy centroid coincides with a region of hot gas likely due to an infalling subcluster.

Coded-mask detectors suppress the flux of diffuse sources and in order to recover the exact source flux and significance one needs to develop dedicated methods for the analysis of extended objects (e.g. Renaud et al. 2006b). Given the fact that Coma is the only cluster ‘resolved’ by BAT, a dedicated analysis will be left to a future paper (Ajello et al. 2008d). However, we can extract the spectrum treating Coma as a point-like source. This translates into an analysis of the source emission within a radius of $10''$ from the BAT centroid. The BAT spectrum is well fitted by a thermal model with gas temperature of $9.13^{+1.68}_{-1.31}$ keV.

XMM-Newton observed Coma several times. We analyzed an observation of 16 ks which took place in June, 2005. The XMM-Newton spectrum was extracted (as described in §2.2) including all photons within $10''$ from the BAT centroid. Integrating the surface brightness profile derived by ROSAT (beta model with $\beta = 0.74$ and core radius $R_c = 10.7''$; Lutovinov et al. 2008) shows that our selection includes $\sim 75\%$ of the total Coma flux. A fit to the XMM-Newton/BAT spectrum with a single temperature model does not yield satisfactory results ($\chi^2/\text{dof} = 1168.9/858$). We then tried to add a power law to the APEC model. Adding a power-law model improves the fit ($\chi^2/\text{dof} = 905.5/856$) and results into a well constrained photon index of $2.11^{+0.11}_{-0.13}$. However, this fit leaves evident (‘snake’-like) residuals at low energy (see below for the residuals of all Coma fits). These residuals might highlight the presence of another thermal component. Indeed, we find that a satisfactory fit ($\chi^2/\text{dof} = 846.5/856$) is achieved using two APEC models. The most intense component has a temperature of $8.40^{+0.25}_{-0.24}$ keV and an abundance of $0.21^{+0.03}_{-0.03}$ consistent with what found by Aumaud et al. (2001) and Lutovinov et al. (2008). The low-temperature component ($T = 1.45^{+0.21}_{-0.11}$ keV and $Z = 0.05^{+0.02}_{-0.02} Z$) accounts very likely for one or more of the X-ray sources in the field of Coma. Indeed, an hardness ratio analysis of these X-ray sources shows

that their spectra are compatible with thermal models with temperatures in the 0.1–2 keV range (Finoguenov et al. 2004). According to Finoguenov et al. (2004), these objects are (non-AGN) galaxies with a suppressed X-ray emission due to reduced star-formation activity. Summarizing, we believe that the double-thermal model explains better the data with respect to the thermal plus power-law model because: 1) it produces the largest improvement in the χ^2 (i.e. largest χ^2_{red}), 2) it better reproduces the low-energy part of the spectrum, and 3) it accounts for all the point-like sources which are present in the XMM-Newton observation. The best fit, sum of two APEC models, is shown in Fig. 6. The residuals to all the fits described in this section are reported in Fig. 7 while their parameters are summarized in Tab. 5.

Our 99% CL upper limit in the 50–100 keV band is $1.70 \times 10^{12} \text{ erg cm}^{-2} \text{ s}^{-1}$. However, we remark that this spectrum is representative only of the 10^0 radius region centered on the BAT centroid. Indeed, since the IC and the thermal emissions are proportional to the electron density and to its square respectively (F_{IC} / n_e and $F_{\text{thermal}} / n_e^2$; e.g. Sarazin et al. 1998a), their ratio (IC/thermal) is expected to increase with the distance from the cluster. Moreover, the lower density and larger sound speed (with respect to the physical conditions in the core) make CR acceleration more efficient in the cluster outskirts (Pfrommer et al. 2007). For these reasons and because Coma is an extended source for BAT, of which we analyze only the core, we cannot exclude the presence of a non-thermal component which arises in the outskirts of the cluster.

2.4.5. Abell 3571

Swift J1347.7–3253 is likely associated with the Abell 3571 cluster, which has also been detected in the RXTE Slow-Survey (Revnivtsev et al. 2004). Its symmetric morphology, see left panel of Fig. 8, and temperature map indicate that A 3571 is a relaxed cluster (e.g. Markevitch et al. 1998). However, the radio structure, of the complex in which A 3571 lays, suggests that this cluster is in the late stages of merging (Venturi et al. 2002). We note that Abell 3571 is known to have a moderate cool core (Peres et al. 1998). Past and recent studies do not report evidences for non-thermal hard X-ray emission in Abell 3571. As to the BAT spectrum with a bremsstrahlung model yields a temperature of $6.9^{+6.0}_{-2.6}$ keV (in agreement with the mean temperature of $6.71^{+0.15}_{-0.42}$ keV measured with Chandra by Sanderson et al. (2006)), but the chi-square ($\chi^2_{\text{red}} = 1.76$) is relatively poor. The BAT spectrum shows positive residuals above 60 keV which might reveal the presence of a hard tail (see Fig. 8). However, given the low S/N of our spectrum, adding a power-law component does not improve the chi-square. XMM-Newton observed Abell 3571 for 12 ks in July, 2007. According Nevalainen et al.

(2001), the surface brightness of Abell 3571 follows a beta profile with $\beta = 0.68$ and core radius $R_c = 3.85''$. Therefore, our region of $10''$ radius includes approximately 93% of the cluster emission. This factor is taken into account when performing the joint fit of XMM-Newton and BAT data. The combined XMM-Newton/BAT spectrum, shown in the right panel of Fig. 8, is well fitted by an APEC model with a plasma temperature of 6.01 ± 0.21 keV and an abundance of 0.34 ± 0.06 solar. The total $2-10$ keV flux of $(8.0 \pm 0.3) \times 10^{-11}$ erg cm $^{-2}$ s $^{-1}$ is in good agreement with the value of $7.3 \pm 0.4 \times 10^{-11}$ erg cm $^{-2}$ s $^{-1}$ measured by BeppoSAX (Nevalainen et al. 2001). Even though statistically not required, a non-thermal power-law (photon index fixed to 2.0) is well constrained by our data. Indeed, we are able to derive a $50-100$ keV flux of $(1.4 \pm 0.5) \times 10^{-12}$ erg cm $^{-2}$ s $^{-1}$.

The radio flux density from the NRAO VLA Sky Survey is $S_{1380 \text{ MHz}} = 8.4$ mJy (Condon et al. 1998). We could not find any reference for the spectral index, so we adopted the value of $\alpha = 1.5$ which leads to the lower limit listed in Table 3. We note that steeper spectrum gives a larger upper limit for the magnetic field (e.g. $\alpha = 2$) would yield a lower limit twice as large as the previous.

2.4.6. Abell 2029

Swift J1511.0+0544 is likely associated with the Abell 2029 cluster, which has also been detected at high energy by RXTE, BeppoSAX and Chandra (Revnivtsev et al. 2004; Molendi & De Grandi 1999; Clarke et al. 2004, respectively). Left panel of Figure 9 shows that the BAT source is well centered on the cluster emission as seen by ROSAT. Abell 2029 has a moderate cool core (Sarazin et al. 1998b; Molendi & De Grandi 1999). Clarke et al. (2004) present an analysis of Chandra observations of the central region and find signs of interactions between the X-ray and the radio plasma. The unusual central radio source (PK S0745-191) morphology would be typical of a merging cluster. They suggest that A 2029 is a cluster that started very recently to cool to lower temperatures.

The BAT data alone are well fit ($\chi^2/\text{dof} = 6.89/10$) by a simple bremsstrahlung model with a temperature of $10.6^{+5.8}_{-3.3}$ keV. An 8 ks long XRT observation took place in September, 2005. Given the extent of the XRT CCD, we extracted all the photons within a $6''$ from the BAT centroid. The surface brightness profile follows a beta model with $\beta = 0.64$ and core radius $R_c = 1.8''$ (Sarazin et al. 1998a). Integrating the beta profile up to $6''$ yields that 95% of the total cluster emission is included in our selection. However, for the case of Abell 2029 the beta profile fails to explain the inner $1.8''$ region which is characterized by a bright core (Sarazin et al. 1998a). Thus, our selection might include an higher fraction of the total cluster emission. Indeed, BAT and XRT data are well fitted without the needs of a

cross-normalization constant. The BAT and XRT data are successfully fitted, by an APEC model with plasma temperature of $7.45^{+0.34}_{-0.34}$ keV and $0.39^{+0.09}_{-0.09}$ solar abundance which is consistent with the Chandra results (Clarke et al. 2004). From the combined fit, we derive a 99% CL upper limit to the non-thermal flux in the 50–100 keV band of 1.27×10^{-12} erg cm⁻² s⁻¹. However, we note that the fit leaves positive residuals at high energy. We thus used a second APEC model, with abundance fixed at 0.4, to account for them. The F-test confirms that the second thermal component is detected at 99.85% CL. The best fit temperatures are $9.6^{+2.0}_{-2.0}$ keV and $4.1^{+1.7}_{-1.5}$ keV respectively. This fit is shown in Fig. 9. Abell 2029 has been targeted by ground-based TeV telescopes; however no TeV emission has been detected so far (Perkins et al. 2006).

Condon et al. (1998) found $S_{1380 \text{ MHz}} = 527.8$ mJy. We adopted the value of $\alpha = 1.5$ which leads to the lower limits on the magnetic field estimated in Table 3. We note that Taylor et al. (1994) obtained a lower limit on the magnetic field of 0.18 G using observations of the central radio galaxy.

2.4.7. Abell 2142

Swift J1558.5+2714 is associated with the Abell 2142 merging cluster. The detection in the 3–20 keV band by RXTE (Revnivtsev et al. 2004) makes the association of the BAT source with the cluster rather strong. According to Peres et al. (1998) and De Grandi & Molendi (2002), Abell 2142 has a cool core that survived the merger. Markevitch et al. (2000) and Sanderson et al. (2006), using Chandra observations, noted that the core of A 2142 has a complex structure, probably with a poor cluster enclosed in the halo of a hotter larger cluster. This would explain the lower temperature in the center, without the presence of a cool core. The left panel of Fig. 10 shows a point-like source located $< 4''$ from the cluster center. This object is the Seyfert 1 galaxy 2E 1556.4+2725. Given the distance, both objects, the cluster and the Sy1, are not separated by BAT.

The BAT data are well fit by a simple bremsstrahlung model ($\chi^2/\text{dof} = 7.96/10$) with plasma temperature of $10.1^{+3.7}_{-2.7}$ keV. We analyzed an XMM-Newton observation of 800 s in conjunction with the BAT data. In this case, we extracted separately the spectrum of the cluster and the spectrum of the Sy1 2E 1556.4+2725. The latter one shows an X-ray spectrum typical of a Sy1 object: i.e. absorption consistent with the Galactic one and photon index of $1.98^{+0.16}_{-0.14}$. The extrapolated flux in the 15–55 keV range is 2.3×10^{-12} erg cm⁻² s⁻¹ and it is well below the BAT sensitivity. Therefore we can consider negligible the Sy1 contribution in the BAT band. The surface brightness of Abell 2142 profile follows a beta model with $\beta = 0.83$ and core radius $R_c = 4.2''$ (Henry & Briel 1996). Integrating the beta

profile up to 10^0 yields that 97% of the total cluster emission is included in our selection. However, for the case of Abell 2142 the beta profile underestimates the brightness of the inner 3^0 region which is characterized by a bright core (Henry & Briel 1996). Thus, our selection might include an higher fraction of the total cluster emission. Indeed, BAT and XMM-Newton BAT spectrum is well fitted by a simple APEC model with a plasma temperature of $8.40^{+0.64}_{-0.45}$ keV. The fit is shown in the right panel of Fig. 10. This is well in agreement with the temperatures of $8.8^{+1.2}_{-0.9}$ keV and 9.0 ± 0.3 keV measured by Chandra and GINGA respectively (Markevitch et al. 2000; White et al. 1994). From our fit the abundance is $0.27^{+0.13}_{-0.13}$ solar. Since no hard X-ray excess is detected, we report 99% CL upper limits. Using a power-law with photon index of 2.0, we derive from the XMM-Newton BAT data a 99% CL upper limit to the 50(100 keV non-thermal flux of $1.6 \cdot 10^{12}$ erg cm⁻² s⁻¹. The 99% CL limit on the non-thermal luminosity is $6.1 \cdot 10^{43}$ erg s⁻¹. The marginal (~ 2) BeppoSAX detection of a non-thermal emission (Nevalainen et al. 2004) is a factor 5 larger than our upper limit and thus incompatible with our data.

The presence of a radio halo was already reported by Harris et al. (1977). Giovannini & Feretti (2000) measured $S_{1400 \text{ MHz}} = 18.3$ mJy. In absence of a measured index we adopt the arbitrary value of $\alpha = 1.5$ to obtain the magnetic field constraint listed in Table 3.

2.4.8. Triangulum Australis

Swift J1638.8-6424, shown in the right panel of Fig. 11, is likely associated with the hot X-ray cluster of galaxies Triangulum Australis. This cluster at $z = 0.058$ has already been detected in the ROSAT, RXTE Slew and INTEGRAL surveys (Voges et al. 1999; Revnivtsev et al. 2004; Stephen et al. 2006). In particular the detections by RXTE and INTEGRAL above 15 keV make this association certain. The Triangulum Australis cluster may host a cool core (Edge et al. 1992; Peres et al. 1998). However, Markevitch et al. (1996) used the temperature and entropy maps from ASCA and ROSAT to find an indication of the probable presence of a subcluster merger and argue that the cool gas in the core does not require a cooling flow. Markevitch et al. (1998) found that a non-thermal component is more likely than a cooling flow.

The BAT spectrum is well fitted ($\chi^2/\text{dof} = 5.68/9$) by a simple bremsstrahlung model with plasma temperature of $13.4^{+6.3}_{-3.7}$ keV. A similar temperature was found by Markevitch et al. (1996) in the centre of the cluster.

XMM-Newton observed the Triangulum Australis cluster for 7480 s in February, 2001.

According to the beta profile reported by Markevitch et al. (1996), selecting photons within 10° of the BAT centroid includes 92% of the cluster emission. We thus employ such cross-normalization factor when fitting XMM-Newton and BAT data. The BAT and XMM-Newton data are consistent with a pure APEC model. From the best fit, shown in the right panel of Fig. 11, we derive a plasma temperature of $9.30^{+0.30}_{-0.30}$ keV and an abundance of $0.30^{+0.07}_{-0.07}$ solar. The XMM-Newton/BAT temperature is in agreement with the mean values of $9.06^{+0.33}_{-0.31}$ keV and 9.50 ± 0.70 keV reported by Ikebe et al. (2002) and by Chen et al. (2007) respectively. Using a power-law with photon index of 2.0, we derive a 99% CL upper limit to non-thermal emission in the 50–100 keV band of 6.5×10^{13} erg cm⁻² s⁻¹.

Condon et al. (1993) report a 4.85 GHz radio source centered $7''$ away from the BAT centroid. They find an upper limit of 33 Jy. We adopt this flux and the arbitrary value of $\alpha = 1.5$ to obtain the magnetic field constraint listed in Table 3.

2.4.9. Ophiucus

Swift J1712.3–2319 lays only 1.7° (see Fig. 12) away from one of the most studied galaxy clusters, Ophiucus, discovered by Johnston et al. (1981). The detection at high-energies by BeppoSAX and INTEGRAL (Nevalainen et al. 2001; Bird et al. 2006, respectively) makes the association with the BAT source certain. Watanabe et al. (2001a) used ASCA to measure the X-ray brightness distribution and temperature map. Considering the similarities with the Coma cluster, they conclude that Ophiucus is not relaxed and has likely experienced a recent merger. The BAT-derived plasma temperature of $9.5^{+1.4}_{-1.1}$ keV is in good agreement with the values of $9.6^{+0.6}_{-0.5}$ keV and $9.0^{+0.3}_{-0.3}$ keV measured by BeppoSAX (Nevalainen et al. 2001) and by Suzaku (Fujita et al. 2008).

A hard X-ray excess was detected by Nevalainen et al. (2001) at a 2 σ level. Very recently, Eckert et al. (2008) using INTEGRAL confirmed this hard X-ray emission at an higher confidence level (4 σ). The imaging capabilities of the instruments on-board INTEGRAL allowed the authors to conclude that the observed excess over the thermal emission is not originating from point sources (such as obscured AGNs) and is therefore non-thermal. This excess is marginally consistent with BAT data. Indeed, from our data we derive a 90% upper limit to the non-thermal component (20–60 keV) of 7.2×10^{12} erg cm⁻² s⁻¹ while the reported non-thermal flux observed by INTEGRAL is $(10.1 \pm 2.5) \times 10^{12}$ erg cm⁻² s⁻¹.

We analyzed an archival Chandra observation of 50 ks. The observation, which took place in October 2002, was performed using the ACIS-S. Given its extent, the Ophiucus cluster is not entirely contained in a single chip. We thus extracted only those photons in a region of radius of 2.1° around the BAT centroid. The region extent is dictated by the size of

the chip. When performing a simultaneous fit with BAT data, we must therefore account for the flux which falls outside of the ACIS-S chip. Assuming that the surface density follows a beta profile and adopting the values of $\beta = 0.64$ and core radius of $R_c = 3.2''$ as found by Watanabe et al. (2001b) and confirmed by Eckert et al. (2008), we derive that only 52% of the total cluster flux is included in our selection. If we let the cross-normalization of the BAT and the Chandra data vary, we derive that the Chandra data show a normalization (with respect the BAT ones) of $53^{+5}_{-6}\%$ which is in good agreement with the 52% derived above. Thus, we fix the cross-normalization factor at 52%. Moreover, as in Blanton et al. (2003) we accounted for the uncertainty in the background subtraction adding a systematic uncertainty of 2%. The joint Chandra/BAT spectrum is well fitted by a single APEC model with a temperature of $9.93^{+0.24}_{-0.24}$ keV and abundance of 0.52 ± 0.03 . Using a power-law with photon index of 2.0, we derive a 99% CL upper limit to the non-thermal emission in the 50{100 keV and 20{60 keV bands of 2.8×10^{12} erg cm⁻² s⁻¹ and 4.5×10^{12} erg cm⁻² s⁻¹ respectively. The INTEGRAL detection is inconsistent ($> 2\sigma$) with our upper limit.

The Ophiucus cluster is associated in the radio domain to the extended radio source MSH 17-203 (Johnston et al. 1981). The most recent radio data date back to 1977 (Slee 1977) and report $S_{160 \text{ MHz}} = 6.4 \text{ Jy}$ and $\alpha = 2$, which we use to produce the lower limit on the magnetic field reported in Tab. 3. The results do not change if we use older radio measurements (e.g. Mills et al. 1960; Jones & Finlay 1974; Slee & Higgins 1975).

2.4.10. Abell 2319

Swift J1920.9+4357 is certainly associated with the massive Abell 2319 cluster, that is undergoing a major merger (e.g. O'Hara et al. 2004). The BAT centroid (see left panel of Fig. 13) lies $2''$ north-west of the peak of the ROSAT emission. Indeed, Chandra observations reveal at the same position a region of hot, $\sim 12 \text{ keV}$, gas while at the position of the ROSAT peak there is likely a cool core (O'Hara et al. 2004). Abell 2319 has been detected above 10 keV by BeppoSAX and RXTE (Molendi et al. 1999; Guber & Rephaeli 2002, respectively). These two measurements are symptomatic of the uncertainty related to the hard X-ray detection claims from non-imaging instruments and the inherent uncertainty from source contamination. Indeed, Molendi & De Grandi (1999) report that no hard-tail emission is present in BeppoSAX data, while Guber & Rephaeli (2002) find that a power-law component can explain some residual features in the 15{30 keV energy range. The BAT data favors the thermal scenario. Indeed the best fit to the data is obtained using a pure bremsstrahlung model with a plasma temperature of $14.1^{+4.0}_{-3.0}$ keV consistent, within the large errors, with the $9.6 \pm 0.3 \text{ keV}$ value measured by BeppoSAX.

In addition, we analyzed a 10 ks XMM-Newton observation together with the BAT data. Utilizing the surface brightness profile obtained by O'Hara et al. (2004) (beta model with $\beta = 0.55$ and core radius $R_c = 2.6''$) we determine that our region of $10''$ radius includes $\sim 90\%$ of the cluster emission. We employ such cross-normalization factor when fitting XMM-Newton and BAT data. The BAT+XMM-Newton spectra, shown in the right panel of Fig. 13, are well fitted by an APEC model with a plasma temperature of $9.27^{+0.27}_{-0.27}$ keV and abundance of $0.25^{+0.04}_{-0.04}$ solar. The 99% upper limit on the 2–10 keV non-thermal flux of 2.70×10^{12} erg cm⁻² s⁻¹ is in disagreement with the non-thermal flux of $(4.0 \pm 0.1) \times 10^{11}$ erg cm⁻² s⁻¹ detected in the same band by RXTE (Grueter & Rephaeli 2002).

Harris & Miley (1978) discovered a diffuse radio halo associated with the A 2319 cluster. An intensive study was done by Feretti et al. (1997), from which we take $S_{610 \text{ MHz}} = 1 \text{ Jy}$ and $\alpha = 0.92$ to estimate the lower limit on the magnetic field reported in Table 3.

3. Cluster Properties

3.1. Constraints on non-thermal excess emission

In order to constrain the non-thermal hard X-ray emission, we have produced 3 σ upper limits on the 50–100 keV non-thermal flux for each source presented in the previous section. We excluded the Perseus and the Coma clusters. Indeed, Perseus is the only cluster where the detected "hard-tail" is certainly produced by the brightest AGN while Coma requires a dedicated analysis. We chose the 50–100 keV energy band because above 50 keV the thermal emission of the clusters is negligible.

The 3 σ upper limit has been computed integrating the source flux in the 50–100 keV range and subtracting the thermal flux arising from the best thermal fit. We added to this value three times the 1 σ uncertainty. The upper limits are reported in Table 3. These upper limits were derived using BAT data alone. It is important to note that, indeed, thanks to the very good sensitivity of BAT, all these upper limits are very stringent. Indeed, the non-thermal flux for all these sources is constrained to be below $\sim 1 \text{ mCrab}$.

In the derivation above, we do not make any assumption on the mechanism generating the non-thermal flux. However, in most cases IC scattering is believed to be the principal emission process (e.g. Sarazin 1999; Nevalainen et al. 2004; Fusco-Femiano et al. 2007; Eckert et al. 2008). If this is true, then the IC emission can be modeled as a power-law with photon index ~ 2 in the 1–200 keV energy range (see e.g. Reimer et al. 2004). We thus computed the 99% CL upper limits to the IC flux in the 50–100 keV band by adding a power-law model to the best fits reported in Tab. 2. These limits are reported in Tab. 4. It

is worth noting that, since we are using XMM-Newton/XRT/Chandra and BAT data, these upper limits are a factor 5{10 lower than those derived using BAT data alone (see Tab. 3).

3.2. Stacking analysis

A few clusters show positive, marginal, residuals above 50 keV; this is the case for Abell 3266, Abell 3571 and Abell 2142. Such features are not statistically significant to warrant an additional component (e.g. non-thermal power-law). However, it might be that the non-thermal component be just below the BAT sensitivity for such clusters. In this case the stacking technique offers the capability to explore the average properties of a given population beyond the current instrumental limit. Thus, we produced the stacked spectrum of all clusters except Perseus and Coma (for the reasons explained above). The average spectrum is produced by the weighted average of all the spectra. The weight is chosen to be the inverse of the variance of a given bin and it is exactly the same procedure used to extract the spectra of each individual source. The same stacking technique has been applied with success to the study of Seyfert galaxies detected by BAT (Ajello et al. 2008c). The total spectrum has an exposure time of 56 Ms and it is shown in Fig. 14. A fit with a simple bremsstrahlung model yields a good chi-square ($\chi^2/\text{dof} = 7.2/10$). The best fit temperature is $10.8^{+0.9}_{-0.8}$ keV which is in very good agreement with the mean temperature of 10.4 keV as determined by averaging the values obtained fitting a simple bremsstrahlung model to each cluster's spectrum (using BAT data alone). This is a good confirmation that the chosen stacking technique reproduces well the average properties of our cluster sample.

From the best thermal fit, we derive a 99% CL upper limit (50{100 keV) for the non-thermal component of $1.9 \cdot 10^{12} \text{ erg cm}^{-2} \text{ s}^{-1}$ (0.3 mCrab). At the average redshift of the sample ($z = 0.058$), this translates into a limiting luminosity of $1.4 \cdot 10^{43} \text{ erg s}^{-1}$. Nevalainen et al. (2004) reported the detection of an average non-thermal component detected in the stacked spectrum (20{80 keV) of BeppoSAX clusters. Their non-thermal luminosity is comprised³ in the $(0.5\{5.0) \cdot 10^{43} \text{ erg s}^{-1}$ range. In the 20{80 keV band our 99% CL limit on the non-thermal luminosity is $2.2 \cdot 10^{43} \text{ erg s}^{-1}$. Thus, the findings of Nevalainen et al. (2004) are consistent with our analysis.

On the other hand, all clusters, except perhaps Perseus and Abell 3571, are undergoing a merging phase. These last two clusters are those which show the lowest ICM temperature in our sample. The $L_x - T$ relation (shown in Fig. 15) reinforces the picture that

³The measurement reported by Nevalainen et al. (2004) had to be converted to the Hubble constant used in this paper.

most of the BAT clusters are mergers. Indeed, the best fit to the data with a power-law of the form $L = A_6 T_6$, where $T_6 = T/6\text{keV}$ (fixed at 2.88^4) yields a normalization $A_6 = (2.82 \pm 0.8) \cdot 10^3 h_{70}^2 \text{ erg s}^{-1}$. While Markevitch (1998) and Aumaud & Evrard (1999), found for A_6 a value of $(12.53 \pm 1.08) \cdot 10^3 h_{70}^2 \text{ erg s}^{-1}$ and $(12.13 \pm 0.06) \cdot 10^3 h_{70}^2 \text{ erg s}^{-1}$ respectively. Indeed, merging clusters are known to segregate at lower luminosities (or higher temperatures) in the $L_x - T$ plane (Ota et al. 2006).

There is a growing evidence which points towards a rather non-uniform distribution of temperatures in the ICM of merging clusters (e.g. Markevitch et al. 2003; O'Hara et al. 2004; Eckert et al. 2007). Both hydrodynamical simulations (e.g. Takizawa 1999) and observations (see Markevitch et al. 2003, for Abell 0754) have shown that shocks due to cluster mergers can heat the ICM up to $\sim 15\text{keV}$. Figure 16 shows that for the merging clusters the mean temperature measured by BAT is slightly larger (given the large uncertainties) than the mean ICM temperature measured below 10keV . A similar trend, although using different wavebands, has been recently reported for a sample of 192 galaxy clusters (Cavagnolo et al. 2008). Moreover, for the merging clusters, the BAT centroid is shifted to positions where Chandra and XMM-Newton have detected regions of hot gas. Based on these evidences, we believe that the conjecture that these clusters show regions of "hot" gas is a more viable claim than the one which foresees the presence of a strong IC component.

This claim is also supported by the fact that the high-energy residuals (e.g. residuals above 10keV of the spectral fits using a single thermal model) are in general better described by an additional thermal component than a power-law model. To prove this, we selected those clusters which show, in the analysis presented in §2.2, the largest residuals above 10keV from the thermal model used. These clusters, which are Abell 2029, Triangulum Australis and Abell 2319, also show a large deviation between the ICM temperature measured below and above 10keV (see Fig. 16). We made a fit to each of these clusters with: 1) a single thermal model, 2) the sum of a thermal and a power-law model, and 3) the sum of two thermal models. The residuals to each of these fits are shown in Figures 17, 18, and 19 while the spectral parameters are summarized in Table 5. We note that in all three cases the additional thermal model explains the residuals better than an additional power-law model. We also remark that for most of the BAT clusters (in this case for Triangulum Australis and Abell 2319) the single thermal model is already a good description of the data ($\chi^2/\text{dof} \approx 1.0$) and given the statistics no other additional model is required. This means that currently the high-energy residuals (with respect a single thermal fit) are not significant. Longer BAT exposures will clarify the existence and nature of these emissions.

⁴ Given the small range in luminosity spanned by our sample we fixed it at the value determined by Aumaud & Evrard (1999).

3.3. Cluster Magnetic Field Assessment

The diffuse synchrotron radio emission (radio halos, relics and mini-halos) proves the existence of magnetic fields in the ICM. The intensity of the synchrotron emission depends both on the strength of the magnetic field and on the electron density. If the non-thermal X-ray emission results from IC scattering of the same radio electrons by the CMB, then the degeneracy in magnetic field and relativistic electron density can be broken (e.g. Rephaeli 2001). Therefore the non-detection of a non-thermal component can be used to place a lower limit on the magnetic fields in clusters (the ratio of IC to radio flux is inversely proportional to B^{-1}). Following Harris & Romaniushin (1974) and Sarazin (1988), we estimate the lower limit on B (the volume averaged component along the line of sight):

$$\frac{f_{x_r}}{s_r} = \frac{2.47 \cdot 10^{19} T_{\text{CMB}}^3 b(p)}{B a(p)} \frac{4960 T_{\text{CMB}}}{B} ; \quad (1)$$

where p is the spectral index, $p = 2 + 1$, f_x the X-ray flux integrated over the band between $\epsilon_{\text{min}} = 50 \text{ KeV}$ and $\epsilon_{\text{max}} = 100 \text{ KeV}$ ($f_x = k_c \int_{\epsilon_{\text{min}}}^{\epsilon_{\text{max}}} \epsilon d\epsilon$, in $\text{erg cm}^{-2} \text{s}^{-1}$), $s_r = k_s \nu$ the flux density at the radio frequency ν (in $\text{erg cm}^{-2} \text{s}^{-1} \text{Hz}^{-1}$), $T_{\text{CMB}} = 2.7 \text{K}$ the temperature of the CMB and $a(p)$ and $b(p)$ as in Sarazin (1988) (eq. 5.6 and 5.8). Since our clusters are nearby, in the formula above we neglect redshift corrections.

Although the limit on the X-ray flux is very stringent, the measurement of the diffuse radio emission is complicated by the presence of individual radio galaxies in the cluster. In most cases the radio observations were not sensitive enough over a wide range of spatial scales to subtract the contribution of the single sources. Moreover, the spectral index varies with the distance from the center of the cluster. These factors make the derivation of the magnetic field intensity uncertain. Therefore the values listed in table 3 have to be taken as order of magnitude estimates. Such estimates point to magnetic fields that are typically a fraction of a G. These low values indicate that these systems are far from equipartition. This is possible if one considers that the magnetic fields and the relativistic particles may have a different spatial extension and history.

The magnetic field can also be evaluated by measuring the Faraday rotation (RM) of the plane of polarization from the radio galaxies in the cluster or in the background (e.g. Kin et al. 1991; Clarke et al. 2001). The two estimates are different (with $B_{\text{RM}} \neq B$), most likely because the interpretation of Faraday rotation measurements and the derivation of the mean magnetic field strength rests on assumptions of the magnetic field topology (see Goldsmith & Rephaeli 1993; Colafrancesco et al. 2005, for an extensive discussion). We can produce a more robust, upper limit on the IC flux considering that the IC emission spectrum

can be approximated as a power law in the 150–200 keV energy band (see e.g. Reimer et al. 2004, for more details). Using both 2–10 keV and BAT data we were able to produce the limits reported in Table 4 which are in some cases a factor 5–10 lower than our previous estimated values (Tab. 3) based on BAT data alone. This in turn translates in larger intensities of the magnetic field which in a few cases reach the 0.5 G value.

4. Cluster Population

4.1. Cluster $\log N - \log S$

Thanks to the serendipitous character of the BAT survey, it is possible to derive, for the first time, the source counts distribution (also known as $\log N - \log S$) of clusters above 15 keV. This can be obtained as:

$$N(>S) = \sum_{i=0}^{N_S} \frac{1}{\Omega_i} \quad [\text{deg}^2] \quad (2)$$

where N_S is the total number of clusters with fluxes greater than S and Ω_i is the geometrical area surveyed to that limiting flux. The cumulative distribution is reported in Fig. 20. Source counts distributions are generally fitted by a power law of the form $N(>S) = AS^{-\alpha}$. Given the small number of objects, we do not attempt a maximum likelihood fit to derive the slope α , but we note that our flux distribution is consistent with an Euclidean function $N/S^{3/2}$ as shown in Fig. 20. We derive the normalization A as that one which reproduces the number of observed objects above the flux of $1 \times 10^{11} \text{ erg cm}^{-2} \text{ s}^{-1}$. Using the 90% confidence limits for small numbers derived by Gehrels (1986), we find that a good representation of our data is obtained by $N(>S) = (4.19^{+2.1}_{-1.4} \times 10^4 \text{ deg}^2) S_{11}^{-1.5}$ where S_{11} is the flux in unit of $10^{11} \text{ erg cm}^{-2} \text{ s}^{-1}$. This function is also shown in Fig. 20.

Interestingly, we note that the integrated flux of all clusters above $10^{11} \text{ erg cm}^{-2} \text{ s}^{-1}$ is $9.7 \times 10^{11} \text{ erg cm}^{-2} \text{ s}^{-1} \text{ sr}^{-1}$. This is only 0.1% of the Cosmic X-ray Background (CXB) flux as measured by BAT in the 15–55 keV band (Ajello et al. 2008b), but 5–10% of the total flux resolved by BAT into AGNs (Ajello et al. 2008c). Thus, clusters of galaxies are a sizable population among the extragalactic objects (mostly AGN) detected by BAT.

We can compare the BAT $\log N - \log S$, with those derived in the 0.5–2 keV band. In doing so, we extrapolate the BAT spectra to the 0.5–2 keV band using the temperatures measured below 10 keV. The cluster surface density above $10^{12} \text{ erg cm}^{-2} \text{ s}^{-1}$ in the 0.5–2.0 keV band is $4.3^{+3.0}_{-2.3} \times 10^2 \text{ deg}^{-2}$ which is in rather good agreement with the finding of Vikhlinin et al. (1998) and Burenin et al. (2007).

The BAT source counts distribution can be used to estimate the foreseen number of galaxy clusters above a given flux limit. In doing so, we adopt for the -1.4 value which has been established by deeper X-ray surveys (e.g. Jones et al. 1998; Bohringer et al. 2001, and references therein). Indeed, using the $-3/2$ value would certainly overestimate the cluster density at lower fluxes. As an example, an instrument surveying the whole sky to 10^{-13} erg $\text{cm}^{-2} \text{s}^{-1}$ would detect approximately 10000 galaxy clusters in the 15{55 keV band. The BAT sample itself will comprise up to 30 objects, if BAT will be able to reach the 0.5 mCrab flux limit on the whole sky.

4.2. X-ray Luminosity Function

Since all our clusters have a measured redshift, we can derive their luminosity function. Its construction relies on the knowledge of the survey volume V_{max} as a function of X-ray luminosity. The survey volume is the volume of the cone defined by the survey area and the luminosity distance at which a cluster with a given luminosity could just be observed at the flux limit. The limiting luminosity distance $D_{L, \text{lim}}$, and thus also V_{max} , can be determined solving iteratively the following equation:

$$D_{L, \text{lim}}^2 = \frac{L_x}{4 F_{\text{lim}} k(T; z)} \quad (3)$$

where L_x is the source luminosity and $k(T; z)$ is the k-correction which accounts for the redshifting of the source spectrum.

Once the V_{max} is computed for each object, the cumulative luminosity function can be derived as:

$$N(> L_x) = \sum_{i=0}^{X^N} \frac{1}{V_{\text{max}}(L_i)} \quad [\text{h}_{70}^3 \text{Mpc}^3]. \quad (4)$$

The cumulative luminosity function of the BAT clusters, obtained with the method reported above, is shown in Fig. 21. Bohringer et al. (2002), analyzing a flux-limited sample of ROSAT galaxy clusters (REFLEX), derived that a good parametrization of the differential luminosity function is a Schechter function of the form:

$$\frac{dN}{dL} = n_0 \exp \left(-\frac{L}{L_*} - \frac{L}{L_*} \right) \frac{1}{L}: \quad (5)$$

In order to compare the REFLEX luminosity function with the BAT one, we adopt for n_0 , L_* and α , the values determined by Bohringer et al. (2002). Moreover, since the REFLEX luminosity function is derived in the 0.1{2.4 keV band, we need to convert the luminosities to

the BAT, 15{55 keV, band. We do this using the mean clusters temperature ($kT = 8.1$ keV) determined in the 2{10 keV band (see right panel of Fig. 16). The reason for adopting this temperature instead of the BAT-derived temperature is double. First, given the S/N ratio, temperatures determined in the 2{10 keV band have a better accuracy than temperatures determined in the BAT band. Most importantly however, using the 2{10 keV temperature allows a more accurate extrapolation of the source luminosity from the ROSAT (0.1{2.4 keV) to the BAT (15{55 keV) band. The extrapolated, cumulative, REFLEX luminosity function is also reported Fig. 21. It is apparent that, notwithstanding the extrapolation, the agreement of the BAT data and the REFLEX luminosity function is excellent. This agreement is not however surprising because most of the BAT clusters constitute the bright end of the REFLEX luminosity function. The value of L converted to the 15{55 keV band is $L = 7.3 \cdot 10^{43} h_{70}^{-1} \text{ erg s}^{-1}$ while $n_0 = 5.13^{+2.7}_{-1.8} \cdot 10^7$ and $\alpha = 1.63$.

Integrating the luminosity function multiplied by the luminosity yields the total X-ray emissivity W of galaxy clusters. Above the survey limit of $2 \cdot 10^{43} \text{ erg s}^{-1}$, we find⁵ $W = 2.83 \cdot 10^{37} \text{ erg s}^{-1} \text{ Mpc}^3$ (15{55 keV). This can be compared to the total emissivity of AGN which was derived for the local Universe and a similar energy band (17{60 keV) by Sazonov et al. (2007). After correcting for the small difference between the energy bands, the AGN local emissivity above $2 \cdot 10^{43} \text{ erg s}^{-1}$ is $W_{\text{AGN}} = 14.1 \cdot 10^{37} \text{ erg s}^{-1} \text{ Mpc}^3$. It is thus clear that galaxy clusters contribute substantially ($\sim 20\%$ level with respect to AGN) to the local X-ray output.

5. Discussion

5.1. Non-thermal hard X-ray emission

Direct evidence of the presence of relativistic electrons in the ICM arises from the existence of large radio halos (Dennison 1980; Feretti & Giovannini 2007). The same electron population responsible for the synchrotron emission can in principle scatter CMB photons by IC and produce hard X-ray radiation. The intensity of this radiation relative to the synchrotron emission ultimately depends on the value of the magnetic field.

A firm detection of non-thermal components in the spectra of galaxy clusters has remained elusive in the past as well as in this study. Indeed, Perseus is the only galaxy cluster in the BAT sample where a non-thermal high-energy component is revealed at high significance. Most likely this component is due to the emission of the central AGN NGC 1275. The

⁵We do not provide an error estimate since the luminosity function was not fitted to the data.

rest of the clusters detected by BAT do not show a significant non-thermal emission. Using BAT data alone, we are able to constrain the non-thermal component below the Crab level in the 50–100 keV energy band. The BeppoSAX detection above 50 keV of an average non-thermal component in the stacked spectrum of several clusters is consistent with the BAT upper limit (Nevalainen et al. 2004). As discussed in § 2.2, some of the individual detections of non-thermal components (e.g. Eckert et al. 2008) are consistent (albeit somewhat marginally) with the upper limits derived using BAT data alone. Thus, we cannot exclude that such non-thermal components exist and that they are currently below or at the limit of the BAT sensitivity. If we assume that the principal emission mechanism is IC scattering of GeV electrons on CMB photons, then the cluster magnetic field is constrained to be < 0.1 G. These low magnetic intensities would show that the magnetic field is far from equipartition (i.e. the energy in the magnetic field is different with respect to the electrons energy). As pointed out by Petrosian & Bykov (2008), this can happen if the sources generating the magnetic field and accelerating the electrons are not identical.

However, IC emission by relativistic electrons can be modeled as a power-law in the 100–200 keV energy regime (e.g. Nevalainen et al. 2004; Reimer et al. 2004). Thus, using XMM-Newton/XRT/Chandra and BAT data we are able to constrain, more robustly, the IC emission mechanism. With this approach, we confirm the detection and the flux of the hard component in the spectrum of Abell 0754, but we are also able to prove (thanks to the resolution of XMM-Newton) that a single point-like object, 2MASX 09091372-0943047, located less than 2° from the BAT centroid accounts for the whole non-thermal emission. For the rest of the clusters, we are able to produce upper limits which are a factor 5–10 lower than previously estimated. These limits in turn translate into a slightly larger intensity of the magnetic field which reduces the gap to Faraday rotation measurements (Kim et al. 1991; Clarke et al. 2001). If the cluster magnetic field is truly of the G order, then the chances of detecting IC emission from clusters with the currently existing instruments become really small (Pfrommer & Enlin 2004). Indeed, the values of the predicted IC flux account for only $< 10\%$ of the claimed non-thermal X-ray emission above 10 keV when taking both primary and secondary-generated electrons into account (see e.g. Miniati et al. 2001). Recently, Pfrommer (2008), using high-resolution simulations of a sample of representative galaxy clusters, showed that the predicted IC flux for the Coma and Perseus clusters would be a factor 50 lower than the claimed detections.

Our combined analysis, thus, put tight constraints on the IC mechanism. However, IC emission is the process that most likely explains the claimed non-thermal emission, but not the only one. Hard X-ray flux from galaxy clusters can be interpreted as bremsstrahlung from supra-thermal electron tail developed in the thermal electron distribution due to stochastic acceleration in the turbulent ICM (e.g. Enlin et al. 1999; Petrosian 2001). In this modeling,

the radio and the non-thermal X-ray flux are no longer strictly related and equipartition may apply. However, the non-thermal bremsstrahlung model requires a continuous input of energy in the ICM which as a consequence will cause its temperature to increase. Thus, the non-thermal bremsstrahlung phase is likely to be short lived (Petrosian & Bykov 2008).

5.2. Structure Formation

All the galaxy clusters detected by BAT, except perhaps Abell 3571, are merging systems. Some, as Abell 0754, Abell 2142 and, Abell 3266, are experiencing violent merging due to encounters of subclusters with comparable masses. In the common scenarios of hierarchical structure formation (e.g. Miniati et al. 2000; Ryu & Kang 2003), large systems evolve as the result of merging of smaller structures. As reviewed in Dolag et al. (2008), cluster mergers generate internal shocks (Mach number less than 4) which provide most of the ICM gas heating (e.g. Quilis et al. 1998), and also likely convert a non-negligible fraction ($\sim 10\%$) of their power into CRs. The shocks primarily heat the ions because the kinetic energy of an ion entering the shock region is larger than that of an electron by their mass ratio (Takizawa 1999). Cosmological simulations have shown (e.g. Pfrommer et al. 2007), that in the case of ongoing merger activity, the relative CR pressure (to the thermal ICM pressure) is greatly enhanced, up to 15{20%, due to strong merger shock waves. This pressure is likely larger in the outskirts of the cluster because of the lower sound speed and the larger density of the ICM in the central region which makes CR acceleration less efficient (Pfrommer et al. 2007).

Hot spots as well as cold fronts have been found in many merging clusters thanks to the superior resolution of Chandra (e.g. Markevitch et al. 2000; Markevitch & Vikhlinin 2001; Markevitch et al. 2003). Hydrodynamical simulations have highlighted that ~ 1 Gyr after the encounter of two clusters with comparable masses post-shock regions with high temperatures ($T \sim 10\text{--}20$ keV) are formed (e.g. Takizawa 1999; Ritchie & Thomas 2002). In the BAT sample there is a clear correlation of gas temperature and merging activity. Indeed, Abell 3571 and Perseus, which are in a late merging stage, display the lowest plasma temperatures among the clusters in our sample. INTEGRAL recently unveiled the presence of a hotter region ($T = 12 \pm 2$ keV) located south-west of the centre of the Coma cluster (Eckert et al. 2007). These findings highlight the important role of merging shocks in the heating of ICM.

5.3. Clusters Statistics

The serendipitous character of the BAT survey allowed us to determine, for the first time above 10 keV, the $\log N - \log S$ and luminosity function distributions of galaxy clusters. Both are in very good agreement with previous studies. The $\log N - \log S$ highlights that the clusters BAT detects produce a negligible fraction ($\sim 0.1\%$) of the X-ray background emission, but they represent a sizable population ($\sim 10\%$) with respect to the local AGN. The BAT $\log N - \log S$ shows that future instruments with a sensitivity 10 or 100 times better than BAT (above 15 keV) will detect clusters at a density of $\sim 0.01 \text{ deg}^{-2}$ and $\sim 0.24 \text{ deg}^{-2}$ respectively.

The BAT luminosity distribution allowed us to determine that the volume emissivity of galaxy clusters is $W(> 2 \times 10^{43} \text{ erg s}^{-1}) = 2.38 \times 10^{-7} \text{ erg s}^{-1} \text{ Mpc}^{-3}$. Above the same limiting luminosity, Sazonov et al. (2007) derived that the volume emissivity of the local AGN is $W_{\text{AGN}} = 14.1 \times 10^{-7} \text{ erg s}^{-1} \text{ Mpc}^{-3}$. Thus, above $2 \times 10^{43} \text{ erg s}^{-1}$, the cluster volume emissivity is 20% of that one of AGN. Integrating the luminosity functions to lower luminosity (e.g. $10^{41} \text{ erg s}^{-1}$) changes this fraction to $\sim 10\%$. This change is due to the fact that at low luminosity the AGN luminosity function is steeper than the cluster luminosity function (e.g. Sazonov et al. 2007; Böhringer et al. 2002).

5.4. Future Prospects

The study of non-thermal processes in clusters of galaxies requires a multi-wavelength approach. The ongoing Swift/BAT survey will likely comprise up to 30 clusters if an all-sky sensitivity of 0.5 mCrab will be reached and it will improve the signal-to-noise ratio for the spectra of the clusters presented here. Ultimately, major progresses are expected with the launch of *Simbol-X*⁶, *XEUS*⁷, *NUSTAR*⁸, and *NEXT*⁹. Indeed, their sensitivities and spectro-imaging capabilities up to high energies (80 keV and beyond) will provide new and better constraints on the hard X-ray emission.

The future generation of radio arrays combined with high-energy observations will allow to shed some light on the energetics of relativistic particles, the nature and frequency of

⁶<http://www.asdc.asi.it/simbol-x/>

⁷<http://www.rssd.esa.int/index.php?project=xeus>

⁸<http://www.nustar.caltech.edu/>

⁹<http://www.astro.isas.ac.jp/future/NEXT/>

acceleration processes, and the strength and structure of magnetic fields. As we already discussed, this astrophysical information has strong cosmological implications. The Long Wavelength Array¹⁰ (LWA), the Low Frequency Array¹¹ (LOFAR), and ultimately the Square Kilometre Array¹² (SKA), will operate over a critical radio frequency range to detect relativistic plasma in large-scale structure and clusters in a sensitive way. The advance in sensitivity and resolution will increase the statistics of known radio halos and radio relics at different redshifts. The correlation of sensitive X-ray and radio detections will be particularly important (e.g. Enlin & Rottgering 2002). At the same time, thanks to the high angular and spectral resolution, the Faraday rotation studies will significantly improve yielding a better determination of the cluster magnetic field.

Much attention is directed towards the Gamma-ray Large Area Space Telescope¹³ (GLAST) which, with an unprecedented sensitivity, spatial resolution and dynamic range at GeV energies, will shed light on the origin of the extragalactic γ -ray background. Galaxy clusters and shocks from structure formations are natural candidates for explaining part of this diffuse emission (e.g. Demer 2007, and references therein). All the BAT clusters are good candidate for GLAST since they are nearby and are mergers. Indeed, in merging systems, part of the internal shocks energy is very likely converted into CRs acceleration (Dolag et al. 2008). As pointed out by Pfister et al. (2008), above 100 MeV the cluster emission will likely be dominated by pion decay γ -rays even though a contribution from non-thermal bremsstrahlung and IC emission of secondary electrons is expected. This will provide a unique information about the hadron component of CRs which is not included in estimates of CR pressure based only on the observations discussed above concerning electrons and magnetic field. Since cosmic ray protons loss time is long, the π^0 -bump detection would proof that hadrons have been confined in the ICM for as long as the Hubble time (e.g. Berezhinsky et al. 1997). Stringent constraints on the cosmic rays content in the ICM is fundamental for the future space missions which will use galaxy clusters to constrain and understand the nature of Dark Energy (e.g. eROSITA¹⁴).

¹⁰<http://lwa.unm.edu>

¹¹<http://www.lofar.org/>

¹²<http://www.skatelescope.org>

¹³<http://www-glast.stanford.edu>

¹⁴<http://www.mpe.mpg.de/projects.html#erোসita>

6. Conclusions

BAT is the first instrument to detect above 15 keV an all-sky sample of galaxy clusters¹⁵. The BAT energy range (15–200 keV) is the best one to investigate the presence of non-thermal emission whose detection remained so far controversial. The results of our investigation can be summarized as follows:

Perseus is the only cluster among the 10 BAT objects which displays an high-energy non-thermal component which extends up to 200 keV. It is very likely that the central AGN NGC 1275 is responsible for such emission. This claim is supported by several evidences: 1) the variability seen with BeppoSAX (Nevalainen et al. 2004), 2) the XMM-Newton spectral analysis (Churazov et al. 2003), and 3) our combined BAT+XRT+XMM-Newton analysis which shows that the nucleus has a typical AGN spectrum.

The BAT spectra of the remaining 9 galaxy clusters is well fitted by a simple thermal model that constrains non-thermal flux to be below 1 mCrab in the 50–100 keV band.

Assuming that IC scattering is the main mechanism at work for producing non-thermal high-energy flux, it is possible to estimate the magnetic field using Radio data and the upper limits derived above. We obtain that in all the BAT clusters the (average) magnetic field is > 0.1 G. These (rather uncertain) values are in disagreement (if the magnetic field intensities are close to the lower limits) with the, also uncertain, Faraday rotation measurements which show that the magnetic field is in the ~ 1 G range. Our low magnetic field values would imply that the magnetic field is far from equipartition.

The stacked spectrum of the BAT clusters (except Perseus and Coma) confirms once again the absence of any non-thermal high-energy component. The 56 Ms stacked spectrum constrains any non-thermal flux to be below 0.3 mCrab (or 1.9×10^{12} erg cm⁻² s⁻¹) in the 50–100 keV band.

Using Swift/XRT, XMM-Newton and Chandra, in addition to BAT data, we were able to produce X-ray cluster spectra which extend more than 3 decades in energy (0.5–50 keV). In all cases, but Perseus and Abell 0754, the broad-band X-ray spectrum is well approximated by a single-temperature thermal model. These spectra allowed us to put constraints on the IC emission mechanism which are a factor > 5 lower than

¹⁵We are aware of an independent work (Okajima et al. 2008) based on an alternative analysis of BAT survey data which reaches conclusions consistent with this analysis.

those derived using BAT data alone. This would in turn imply a larger intensity of the magnetic field. For both Perseus and Abell 0754 an additional power-law component is statistically required, but several evidences confirm that two X-ray point sources (NGC 1275 and 2MASX 09091372-0943047) account for the total non-thermal emission.

The cluster centroid shift in different wavebands, the morphology and the complex temperature maps (available in literature), show that 8 out of 10 clusters are in the middle of a major merging phase. Shocks, which are revealed by XMM-Newton and Chandra images, are actively heating the ICM as the BAT high temperatures testify. The BAT observations and limits on the non-thermal emissions can help to calibrate the large scale structure formation simulations focusing in particular on the treatment of non-thermal particle emission and cooling.

We have produced the first cluster source count (also known as $\log N - \log S$) distribution above 15 keV. This shows that, at the limiting fluxes sampled by BAT, the surface density of clusters is 5% of that one of AGNs. Moreover, we find that the contribution of clusters to the Cosmic X-ray background is of the 0.1% order in the 15-55 keV band. The BAT $\log N - \log S$ can be used to predict the cluster surface density for future hard X-ray instruments.

The X-ray luminosity function of the BAT clusters, the first derived above 15 keV, is in excellent agreement with the ROSAT luminosity function derived in the 0.1-2.4 keV band.

MA acknowledges funding from the DFG Leibniz-Prize (HA 1850/28-1). PR is supported by the Pappalardo Postdoctoral Fellowship in Physics at MIT. NC was partially supported from a NASA grant NNX07AV03G. MA and PR wish to acknowledge Balu for his incomparable constant enthusiasm. We thank T. Okajima for providing a copy of his manuscript before submission and for interesting discussions. The anonymous referee is acknowledged for his helpful comments which improved the manuscript. This research has made use of the NASA/IPAC extragalactic Database (NED) which is operated by the Jet Propulsion Laboratory, of data obtained from the High Energy Astrophysics Science Archive Research Center (HEASARC) provided by NASA's Goddard Space Flight Center, of the SIMBAD Astronomical Database which is operated by the Centre de Données astronomiques de Strasbourg, and of the ROSAT All Sky Survey maintained by the Max Planck Institut für Extraterrestrische Physik.

Facilities: Swift (BAT/XRT), XMM-Newton, Chandra.

REFERENCES

- Ajello, M., Greiner, J., Kanbach, G., Rau, A., Strong, A.W., & Kennea, J.A. 2008a, *ApJ*, 678, 102
- Ajello, M., Greiner, J., Sato, G., & Kanbach, G. 2008b, *ApJ*, submitted
- Ajello, M., Rau, A., Greiner, J., Kanbach, G., Salvato, M., Strong, A.W., Barthelmy, S.D., Gehrels, N., Markwardt, C.B., & Tueller, J. 2008c, *ApJ*, 673, 96
- Ajello, M., Rebusco, P., Cappelluti, N., Greiner, J., & Reimer, O. 2008d, (in preparation)
- Anders, E. & Grevesse, N. 1989, *Geochim. Cosmochim. Acta*, 53, 197
- Ando, S. & Nagai, D. 2007, *ArXiv e-prints*, 705
- Aumaud, M., Aghanim, N., Gastaud, R., Neumann, D.M., Lumb, D., Briel, U., Altieri, B., Ghizzardi, S., Mottaz, J., Sasseen, T.P., & Vestrand, W.T. 2001, *A & A*, 365, L67
- Aumaud, M. & Evrard, A.E. 1999, *MNRAS*, 305, 631
- Avni, Y. 1976, *ApJ*, 210, 642
- Bacchi, M., Feretti, L., Giovannini, G., & Govoni, F. 2003, *A & A*, 400, 465
- Barthelmy, S.D., Barbier, L.M., Cummings, J.R., Fenimore, E.E., Gehrels, N., Hullinger, D., Krimm, H.A., Markwardt, C.B., Palmer, D.M., Parsons, A., Sato, G., Suzuki, M., Takahashi, T., Tashiro, M., & Tueller, J. 2005, *Space Science Reviews*, 120, 143
- Berezinsky, V.S., Blasi, P., & Ptuskin, V.S. 1997, *ApJ*, 487, 529
- Bird, A.J., Barlow, E.J., Bassani, L., Bazzano, A., Belanger, G., Bodaghee, A., Capitanio, F., Dean, A.J., Focchi, M., Hill, A.B., Lebrun, F., Malizia, A., Mas-Hesse, J.M., Molina, M., Moran, L., Renaud, M., Sguera, V., Shaw, S.E., Stephen, J.B., Terrier, R., Ubertini, P., Walter, R., Willis, D.R., & Winkler, C. 2006, *ApJ*, 636, 765
- Blanton, E.L., Sarazin, C.L., & McNamara, B.R. 2003, *ApJ*, 585, 227
- Blasi, P., Gabici, S., & Brunetti, G. 2007, *ArXiv Astrophysics e-prints*
- Bohringer, H., Collins, C.A., Guzzo, L., Schuecker, P., Voges, W., Neumann, D.M., Schindler, S., Chincarini, G., DeGrandi, S., Cudde, R.G., Edge, A.C., Reiprich, T.H., & Shaver, P. 2002, *ApJ*, 566, 93

- Bohringer, H ., Schuecker, P ., Guzzo, L ., Collins, C .A ., Voges, W ., Schindler, S ., Neumann, D .M ., Cruddace, R .G ., De Grandi, S ., Chincarini, G ., Edge, A .C ., McGillivray, H .T ., & Shaver, P . 2001, *A & A* , 369, 826
- Bonamente, M ., Liu, R ., & Mitaz, J .P .D . 2001, *ApJ* , 561, L63
- Bowyer, S ., Berghofer, T .W ., & Korpela, E .J . 1999, *ApJ* , 526, 592
- Brown, D .L . & Burns, J .O . 1991, *AJ* , 102, 1917
- Brunetti, G ., Blasi, P ., Cassano, R ., & Gabici, S . 2004, *MNRAS* , 350, 1174
- Burenin, R .A ., Vikhlinin, A ., Homstrup, A ., Ebeling, H ., Quintana, H ., & Meshcheryakov, A . 2007, *ApJS* , 172, 561
- Bykov, A .M ., Blomen, H ., & Uvarov, Y .A . 2000, *A & A* , 362, 886
- Catura, R .C ., Fisher, P .C ., Johnson, H .M ., & Meyerott, A .J . 1972, *ApJ* , 177, L1
- Cavagnolo, K .W ., Donahue, M ., Voit, M ., & Sun, M . 2008, *ApJ* (accepted)
- Chen, Y ., Reiprich, T .H ., Bohringer, H ., Ikebe, Y ., & Zhang, Y .-Y . 2007, *A & A* , 466, 805
- Churazov, E ., Forman, W ., Jones, C ., & Bohringer, H . 2003, *ApJ* , 590, 225
- Churazov, E ., Forman, W ., Vikhlinin, A ., Tremaine, S ., Gerhard, O ., & Jones, C . 2007, *ArXiv eprints* , 711
- Clarke, T .E ., Blanton, E .L ., & Sarazin, C .L . 2004, *ApJ* , 616, 178
- Clarke, T .E ., Kronberg, P .P ., & Bohringer, H . 2001, *ApJ* , 547, L111
- Colafrancesco, S ., Marchegiani, P ., & Perola, G .C . 2005, *A & A* , 443, 1
- Condon, J .J ., Cotton, W .D ., Geisen, E .W ., Yin, Q .F ., Perley, R .A ., Taylor, G .B ., & Boderick, J .J . 1998, *AJ* , 115, 1693
- Condon, J .J ., Grith, M .R ., & Wright, A .E . 1993, *AJ* , 106, 1095
- Dar, A . & Shaviv, N .J . 1995, *Physical Review Letters* , 75, 3052
- De Grandi, S . & Molendi, S . 1999, *ApJ* , 527, L25
- | . 2002, *ApJ* , 567, 163

- de Plaa, J., Werner, N., Bykov, A. M., Kaastra, J. S., Mendez, M., Vink, J., Bleeker, J. A. M., Bonamente, M., & Peterson, J. R. 2006, *A & A*, 452, 397
- Dennison, B. 1980, *ApJ*, 239, L93
- Demmer, C. D. 2007, *ApJ*, 659, 958
- Dolag, K., Bykov, A. M., & Diaferio, A. 2008, *Space Science Reviews*, 29
- Durret, F., Slezak, E., Lieu, R., Dos Santos, S., & Bonamente, M. 2002, *A & A*, 390, 397
- Ebisawa, K., Bourban, G., Bodaghee, A., Molavi, N., & Courvoisier, T. J.-L. 2003, *A & A*, 411, L59
- Eckert, D., Produit, N., Neronov, A., & Courvoisier, T. J. 2007, *ArXiv e-prints*, 710
- Eckert, D., Produit, N., Paltani, S., Neronov, A., & Courvoisier, T. J.-L. 2008, *A & A*, 479, 27
- Edge, A. C., Stewart, G. C., & Fabian, A. C. 1992, *MNRAS*, 258, 177
- Ensslin, T. A., Biermann, P. L., Kronberg, P. P., & Wu, X.-P. 1997, *ApJ*, 477, 560
- Enlin, T. A., Lieu, R., & Biermann, P. L. 1999, *A & A*, 344, 409
- Enlin, T. A. & Rottgering, H. 2002, *A & A*, 396, 83
- Ettori, S., Fabian, A. C., & White, D. A. 1998, *MNRAS*, 300, 837
- Fabian, A. C., Pringle, J. E., & Rees, M. J. 1976, *Nature*, 263, 301
- Felten, J. E., Gould, R. J., Stein, W. A., & Wolf, N. J. 1966, *ApJ*, 146, 955
- Feretti, L. & Giovannini, G. 1998, in *Untangling Coma Berenices: A New Vision of an Old Cluster*, ed. A. M. Azure, F. Casoli, F. Durret, & D. Gerbal, 123{+
- Feretti, L. & Giovannini, G. 2007, preprint (astro-ph/0703494)
- Feretti, L., Giovannini, G., & Bohringer, H. 1997, *New Astronomy*, 2, 501
- Finoguenov, A., Briel, U. G., Henry, J. P., Gavazzi, G., Iglesias-Paramo, J., & Boselli, A. 2004, *A & A*, 419, 47
- Finoguenov, A., Henriksen, M. J., Miniati, F., Briel, U. G., & Jones, C. 2006, *ApJ*, 643, 790
- Forman, W., Kellogg, E., Gursky, H., Tananbaum, H., & Giacconi, R. 1972, *ApJ*, 178, 309

- Fritz, G ., Davidse, A ., Meekins, J.F ., & Friedman, H .1971, ApJ, 164, L81
- Fujita, Y ., Hayashida, K ., Nagai, M ., Inoue, S ., Matsumoto, H ., Okabe, N ., Reiprich, T .H ., Sarazin, C .L ., & Takizawa, M .2008, A&A e-prints, 806
- Fujita, Y ., Kohri, K ., Yamazaki, R ., & Kino, M .2007, ApJ, 663, L61
- Fujita, Y ., Takizawa, M ., & Sarazin, C .L .2003, ApJ, 584, 190
- Fusco-Femiano, R ., dalFiume, D ., Feretti, L ., Giovannini, G ., Grandi, P ., Matt, G ., Molendi, S ., & Santangelo, A .1999, ApJ, 513, L21
- Fusco-Femiano, R ., Landi, R ., & Orlandini, M .2007, ApJ, 654, L9
- Fusco-Femiano, R ., Orlandini, M ., Brunetti, G ., Feretti, L ., Giovannini, G ., Grandi, P ., & Setti, G .2004, ApJ, 602, L73
- Fusco-Femiano, R ., Orlandini, M ., De Grandi, S ., Molendi, S ., Feretti, L ., Giovannini, G ., Bacchi, M ., & Govoni, F .2003, A&A, 398, 441
- Gehrels, N .1986, ApJ, 303, 336
- Gehrels, N ., Chincarini, G ., Giommi, P ., Mason, K .O ., Nousek, J.A ., Wells, A .A ., White, N .E ., Barthelmy, S.D ., Burrows, D .N ., Cominsky, L.R ., Hurley, K .C ., Marshall, F.E ., Meszaros, P ., Roming, P.W .A ., Angelini, L ., Barbier, L.M ., Belloni, T ., Campana, S ., Caraveo, P.A ., Chester, M.M ., Citterio, O ., Cline, T.L ., Cropper, M.S ., Cummings, J.R ., Dean, A.J ., Feigelson, E.D ., Fenimore, E.E ., Frail, D.A ., Fruchter, A.S ., Garmire, G.P ., Gendreau, K ., Ghisellini, G ., Greiner, J., Hill, J.E ., Hunsberger, S.D ., Krimm, H.A ., Kulkarni, S.R ., Kumar, P ., Lebrun, F ., Lloyd-Ronning, N.M ., Markwardt, C.B ., Mattson, B.J ., Moshotzky, R.F ., Norris, J.P ., Osborne, J., Paczynski, B ., Palmer, D.M ., Park, H.S ., Parsons, A.M ., Paul, J., Rees, M.J ., Reynolds, C.S ., Rhoads, J.E ., Sassee, T.P ., Schaefer, B.E ., Short, A.T ., Smale, A.P ., Smith, I.A ., Stella, L ., Tagliaferri, G ., Takahashi, T ., Tashiro, M ., Townsley, L.K ., Tueller, J., Turner, M.J.L ., Vietri, M ., Voges, W ., Ward, M.J ., Willingale, R ., Zerbi, F.M ., & Zhang, W.W .2004, ApJ, 611, 1005
- Giacconi, R ., Murray, S., Gursky, H ., Kellogg, E ., Schreier, E ., & Tananbaum, H .1972, ApJ, 178, 281
- Giovannini, G . & Feretti, L .2000, New Astronomy, 5, 335
- Giovannini, G ., Feretti, L ., Venturi, T ., Kin, K.-T ., & Kronberg, P.P .1993, ApJ, 406, 399

- Gisler, G. R. & Miley, G. K. 1979, *A & A*, 76, 109
- Gitti, M., Brunetti, G., & Setti, G. 2002, *A & A*, 386, 456
- Goldsmith, O. & Rephaeli, Y. 1993, *ApJ*, 411, 518
- Gruher, D. & Rephaeli, Y. 2002, *ApJ*, 565, 877
- Harris, D. E., Bahcall, N. A., & Strom, R. G. 1977, *A & A*, 60, 27
- Harris, D. E. & Miley, G. K. 1978, *A & AS*, 34, 117
- Harris, D. E. & Romaniushin, W. 1974, *ApJ*, 188, 209
- Henriksen, M. J. & Markevitch, M. L. 1996, *ApJ*, 466, L79
- Henry, J. P. & Briel, U. G. 1995, *ApJ*, 443, L9
- | .1996, *ApJ*, 472, 137
- Henry, J. P., Finoguenov, A., & Briel, U. G. 2004, *ApJ*, 615, 181
- Ikebe, Y., Reiprich, T. H., Bohringer, H., Tanaka, Y., & Kitayama, T. 2002, *A & A*, 383, 773
- Inoue, S., Aharonian, F. A., & Sugiyama, N. 2005, *ApJ*, 628, L9
- Johnston, M. D., Bradt, H. V., Dossay, R. E., Marshall, F. E., Schwartz, D. A., & Margon, B. 1981, *ApJ*, 245, 799
- Jones, B. B. & Finlay, E. A. 1974, *Australian Journal of Physics*, 27, 687
- Jones, L. R., Scharf, C., Ebeling, H., Perlman, E., Wegner, G., Malkan, M., & Homer, D. 1998, *ApJ*, 495, 100
- Kaasra, J. S., Bykov, A. M., Schindler, S., Bleeker, J. A. M., Borgani, S., Diaferio, A., Dolag, K., Durret, F., Nevalainen, J., Ohashi, T., Paerels, F. B. S., Petrosian, V., Rephaeli, Y., Richter, P., Schaye, J., & Wemer, N. 2008, *Space Science Reviews*, 36
- Katz, J. I. 1976, *ApJ*, 207, 25
- Kempner, J. C. & Sarazin, C. L. 2001, *ApJ*, 548, 639
- Kennea, J. A., Markwardt, C. B., Tueller, J., Barthelmy, S., Burrows, D., Campana, S., Falcone, A., Gehrels, N., Grupe, D., Godet O., Krimm, H., Mangano, V., Mineo, T., Pagnani, C., Page, K., Mushotzky, R. F., & Skinner, G. K. 2005, *The Astronomer's Telegram*, 677, 1

- Kin, K.-T., Kronberg, P.P., & Tribble, P.C. 1991, *ApJ*, 379, 80
- Lieu, R., Mittaz, J.P.D., Bowyer, S., Lockman, F.J., Hwang, C.-Y., & Schmitt, J.H.M.M. 1996, *ApJ*, 458, L5
- Lumb, D.H., Warwick, R.S., Page, M., & De Luca, A. 2002, *A & A*, 389, 93
- Lutovinov, A.A., Vikhlinin, A., Churazov, E.M., Revnivtsev, M.G., & Sunyaev, R.A. 2008, *arXiv e-prints*, 802
- Markevitch, M. 1998, *ApJ*, 504, 27
- Markevitch, M., Forman, W.R., Sarazin, C.L., & Vikhlinin, A. 1998, *ApJ*, 503, 77
- Markevitch, M., Mazzotta, P., Vikhlinin, A., Burke, D., Butt, Y., David, L., Donnelly, H., Forman, W.R., Harris, D., Kin, D.-W., Virani, S., & Vrtilek, J. 2003, *ApJ*, 586, L19
- Markevitch, M., Ponman, T.J., Nulsen, P.E.J., Bautz, M.W., Burke, D.J., David, L.P., Davis, D., Donnelly, R.H., Forman, W.R., Jones, C., Kaastra, J., Kellogg, E., Kin, D.-W., Kolodziejczak, J., Mazzotta, P., Pagliaro, A., Patel, S., Van Speybroeck, L., Vikhlinin, A., Vrtilek, J., Wise, M., & Zhao, P. 2000, *ApJ*, 541, 542
- Markevitch, M. & Vikhlinin, A. 2001, *ApJ*, 563, 95
- Markevitch, M.L., Sarazin, C.L., & Irwin, J.A. 1996, *ApJ*, 472, L17
- Markwardt, C.B., Tueller, J., Skinner, G.K., Gehrels, N., Barthelmy, S.D., & Mushotzky, R.F. 2005, *ApJ*, 633, L77
- Mills, B.Y., Slee, O.B., & Hill, E.R. 1960, *Australian Journal of Physics*, 13, 676
- Miniati, F., Jones, T.W., Kang, H., & Ryu, D. 2001, *ApJ*, 562, 233
- Miniati, F., Ryu, D., Kang, H., Jones, T.W., Cen, R., & Ostriker, J.P. 2000, *ApJ*, 542, 608
- Miralda-Escude, J. & Babul, A. 1995, *ApJ*, 449, 18
- Molendi, S. & De Grandi, S. 1999, *A & A*, 351, L41
- Molendi, S., de Grandi, S., Fusco-Femiano, R., Colafrancesco, S., Fiore, F., Nesci, R., & Tamburelli, F. 1999, *ApJ*, 525, L73
- Molendi, S. & Gastaldello, F. 2008, *arXiv:0807.2653*
- Nagai, D., Vikhlinin, A., & Kravtsov, A.V. 2007, *ApJ*, 655, 98

- Nevalainen, J., Kaastra, J., Parmar, A. N., Markevitch, M., Osterbroek, T., Colafrancesco, S., & Mazzotta, P. 2001, *A & A*, 369, 459
- Nevalainen, J., Osterbroek, T., Bonamente, M., & Colafrancesco, S. 2004, *ApJ*, 608, 166
- O'Hara, T. B., Mohr, J. J., & Guerrero, M. A. 2004, *ApJ*, 604, 604
- Okajima, T., Tueller, J., & Gehrels, N. 2008, (in preparation)
- Ota, N., Kitayama, T., Masai, K., & Mitsuda, K. 2006, *ApJ*, 640, 673
- Peres, C. B., Fabian, A. C., Edge, A. C., Allen, S. W., Johnstone, R. M., & White, D. A. 1998, *MNRAS*, 298, 416
- Perkins, J. S., Badran, H. M., Blaylock, G., Bradbury, S. M., Cogan, P., Chow, Y. C. K., Cui, W., Daniel, M. K., Falcone, A. D., Fegan, S. J., Finley, J. P., Fortin, P., Fortson, L. F., Gillanders, G. H., Gutierrez, K. J., Grube, J., Hall, J., Hanna, D., Holder, J., Horan, D., Hughes, S. B., Humensky, T. B., Kenny, G. E., Kertzman, M., Kieda, D. B., Kildea, J., Kosack, K., Krawczynski, H., Krennrich, F., Lang, M. J., LeBohec, S., Maier, G., Moriarty, P., Ong, R. A., Pohl, M., Ragan, K., Rebillot, P. F., Sembroski, G. H., Steele, D., Swordy, S. P., Valcarcel, L., Vassiliev, V. V., Wakely, S. P., Weekes, T. C., & Williams, D. A. 2006, *ApJ*, 644, 148
- Petrosian, V. 2001, *ApJ*, 557, 560
- Petrosian, V. & Bykov, A. M. 2008, *Space Science Reviews*, 25
- Pfrommer, C. 2008, *MNRAS*, 385, 1242
- Pfrommer, C. & Enlin, T. A. 2004, *A & A*, 413, 17
- Pfrommer, C., Enlin, T. A., & Springel, V. 2008, *MNRAS*, 277
- Pfrommer, C., Enlin, T. A., Springel, V., Jubelgas, M., & Dolag, K. 2007, *MNRAS*, 378, 385
- Primini, F. A., Basinska, E., Howe, S. K., Lang, F., Levine, A. M., Lewin, W. H. G., Rothschild, R., Baity, W. A., Gruber, D. E., Knight, F. K., Matteson, J. L., Lea, S. M., & Reichert, G. A. 1981, *ApJ*, 243, L13
- Quilis, V., Ibanez, J. M. A., & Saez, D. 1998, *ApJ*, 502, 518
- Read, A. M. & Ponman, T. J. 2003, *A & A*, 409, 395

- Reimer, A., Reimer, O., Schlickeiser, R., & Iyudin, A. 2004, *A & A*, 424, 773
- Reimer, O., Pohl, M., Sreekumar, P., & Mattox, J.R. 2003, *ApJ*, 588, 155
- Renaud, M., Belanger, G., Paul, J., Lebrun, F., & Terrier, R. 2006a, *A & A*, 453, L5
- Renaud, M., Gros, A., Lebrun, F., Terrier, R., Goldwurm, A., Reynolds, S., & Kalemci, E. 2006b, *A & A*, 456, 389
- Raphaeli, Y. 1979, *ApJ*, 227, 364
- Raphaeli, Y. 2001, in *American Institute of Physics Conference Series*, Vol. 558, American Institute of Physics Conference Series, ed. F.A. Aharonian & H.J. Volk, 427
- Raphaeli, Y. & Gruber, D. 2002, *ApJ*, 579, 587
- Raphaeli, Y., Nevalainen, J., Ohashi, T., & Bykov, A.M. 2008, *Space Science Reviews*, 134, 71
- Revnivtsev, M., Sazonov, S., Jahoda, K., & Gilfanov, M. 2004, *A & A*, 418, 927
- Ritchie, B.W. & Thomas, P.A. 2002, *MNRAS*, 329, 675
- Robertson, J.G. & Roach, G.J. 1990, *MNRAS*, 247, 387
- Rossetti, M. & Molendi, S. 2004, *A & A*, 414, L41
- . 2007, preprint (astro-ph/0702417)
- Ryu, D. & Kang, H. 2003, *Journal of Korean Astronomical Society*, 36, 105
- Sanders, J.S. & Fabian, A.C. 2007, *MNRAS*, 381, 1381
- Sanders, J.S., Fabian, A.C., Allen, S.W., & Schmidt, R.W. 2004, *MNRAS*, 349, 952
- Sanders, J.S., Fabian, A.C., & Dunn, R.J.H. 2005, *MNRAS*, 360, 133
- Sanderson, A.J.R., Ponman, T.J., & O'Sullivan, E. 2006, *MNRAS*, 372, 1496
- Sarazin, C.L. 1988, *X-ray emission from clusters of galaxies* (Cambridge Astrophysics Series, Cambridge: Cambridge University Press, 1988)
- . 1999, *ApJ*, 520, 529
- Sarazin, C.L. & Kempner, J.C. 2000, *ApJ*, 533, 73

- Sarazin, C. L., Wise, M. W., & Markevitch, M. L. 1998a, *ApJ*, 498, 606
- | . 1998b, *ApJ*, 498, 606
- Sauvageot, J. L., Belsole, E., & Pratt, G. W. 2005, *A & A*, 444, 673
- Sazonov, S., Revnivtsev, M., Krivonos, R., Churazov, E., & Sunyaev, R. 2007, *A & A*, 462, 57
- Slee, O. B. 1977, *Australian Journal of Physics Astrophysical Supplement*, 43, 1
- Slee, O. B. & Higgins, C. S. 1975, *Australian Journal of Physics Astrophysical Supplement*, 36, 1
- Smith, R. K., Brickhouse, N. S., Liedahl, D. A., & Raymond, J. C. 2001, *ApJ*, 556, L91
- Stephen, J. B., Bassani, L., Malizia, A., Bazzano, A., Ubertini, P., Bird, A. J., Dean, A. J., Lebrun, F., & Walter, R. 2006, *A & A*, 445, 869
- Takizawa, M. 1999, *ApJ*, 520, 514
- Taylor, G. B., Barton, E. J., & Ge, J. 1994, *AJ*, 107, 1942
- Thierbach, M., Klein, U., & Wiebink, R. 2003, *A & A*, 397, 53
- Timokhin, A. N., Aharonian, F. A., & Neronov, A. Y. 2004, *A & A*, 417, 391
- Tueller, J., Barthelmy, S., Burrows, D., Falcone, A., Gehrels, N., Grupe, D., Kennea, J., Markwardt, C. B., Moshotzky, R. F., & Skinner, G. K. 2005a, *The Astronomer's Telegram*, 668, 1
- | . 2005b, *The Astronomer's Telegram*, 669, 1
- Valinia, A., Henriksen, M. J., Loewenstein, M., Roettiger, K., Moshotzky, R. F., & Madejski, G. 1999, *ApJ*, 515, 42
- Venturi, T., Bardelli, S., Zagaria, M., Prandoni, I., & Morganti, R. 2002, *A & A*, 385, 39
- Vikhlinin, A., McNamara, B. R., Forman, W., Jones, C., Quintana, H., & Homstrip, A. 1998, *ApJ*, 498, L21
- Voges, W., Aschenbach, B., Boller, T., Brauning, H., Briel, U., Burkert, W., Dennerl, K., Englhauser, J., Gruber, R., Haberl, F., Hartner, G., Hasinger, G., Kurster, M., Pfeiffermann, E., Pietsch, W., Predehl, P., Rosso, C., Schmitt, J. H. M. M., Trümper, J., & Zimmernann, H. U. 1999, *A & A*, 349, 389

W atanabe, M ., Yam ashita, K ., Funuzawa, A ., K unieda, H ., & Tawara, Y . 2001a, PA SJ, 53, 605

| . 2001b, PA SJ, 53, 605

W emer, N ., K aastra, J. S., Takei, Y ., Lieu, R ., V ink, J., & Tam ura, T . 2007, A & A , 468, 849

W hite, III, R . E ., Day, C . S. R ., Hatsukade, I., & Hughes, J. P . 1994, A pJ, 433, 583

W illson, M . A . G . 1970, M NRAS, 151, 1

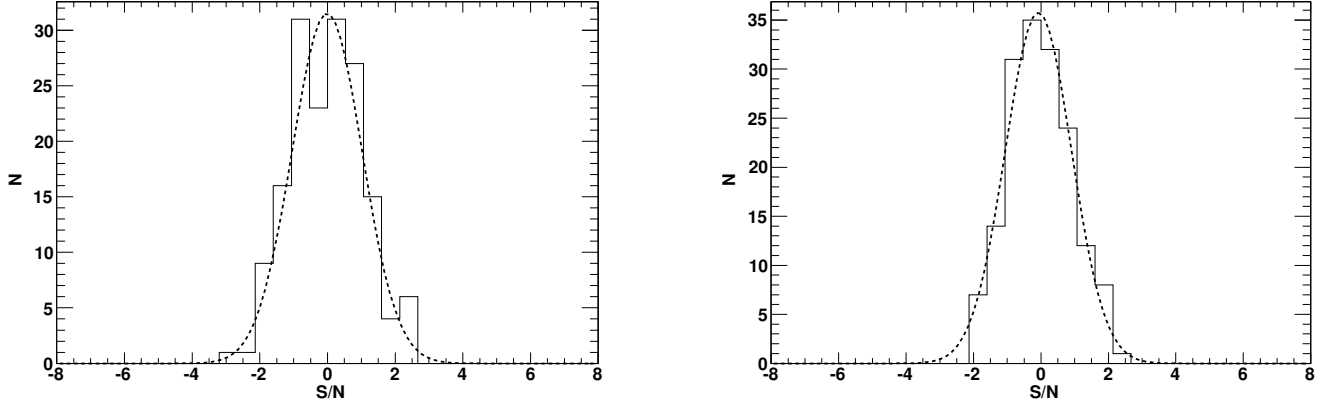


Fig. 1. | Assessment of systematic errors for two representative energy channels: 18.22 keV (left) and 57.6/75.4 keV (right). The histograms show the distribution of S/N for 160 random positions (noise) in the sky away from known or detected sources. The dashed line is a fit to the data using a Gaussian profile. The 1 σ widths of the Gaussian profiles are compatible with 1.0.

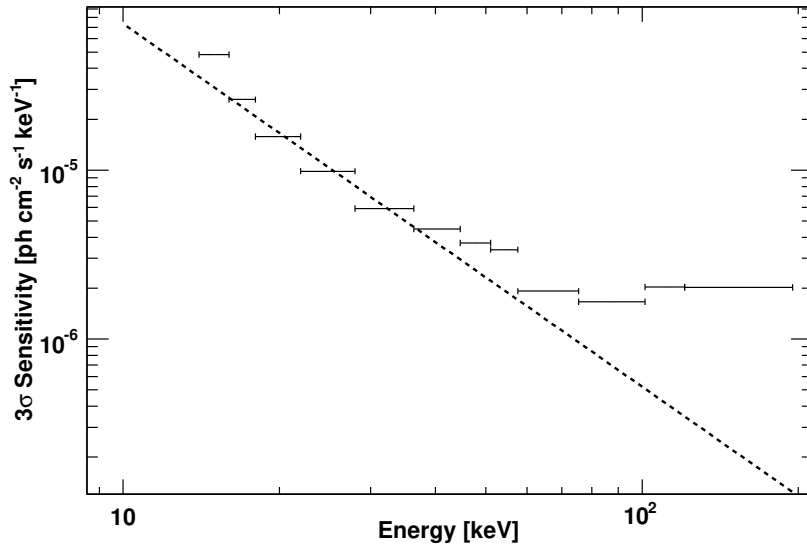


Fig. 2. | 3 σ average spectral sensitivity as a function of energy based on the analysis of 160 randomly extracted spectra. The dashed line is the Crab Nebula spectrum divided by 1000.

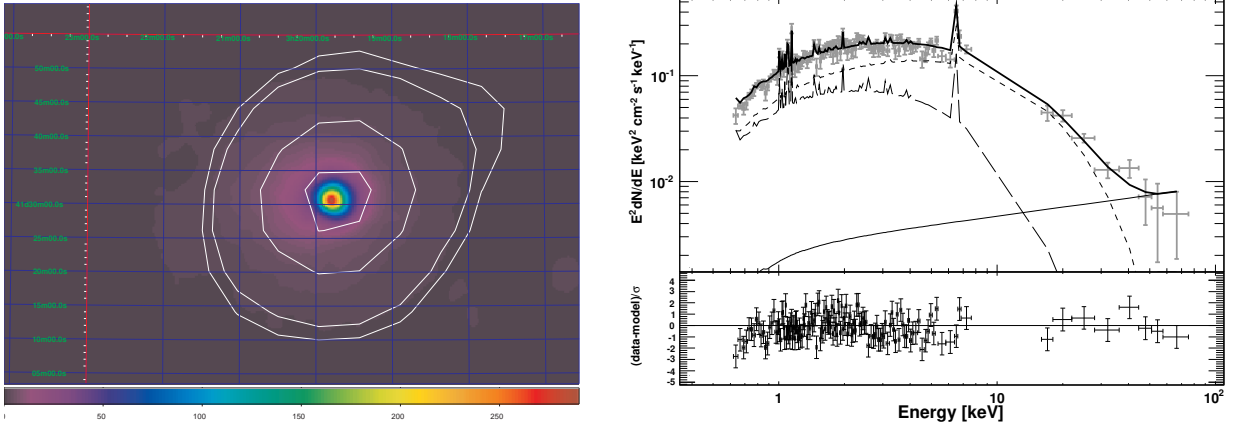


Fig. 3. Left Panel: ROSAT 0.1{2.4 keV surface brightness of Perseus with BAT significance contours superimposed. The contours range from 2.5 to 28. Right Panel: Joint XRT{BAT spectrum of Perseus. The best fit (thick solid line) is the sum of two thermal models (dashed and long-dashed line) and of a power-law component (thin solid line).

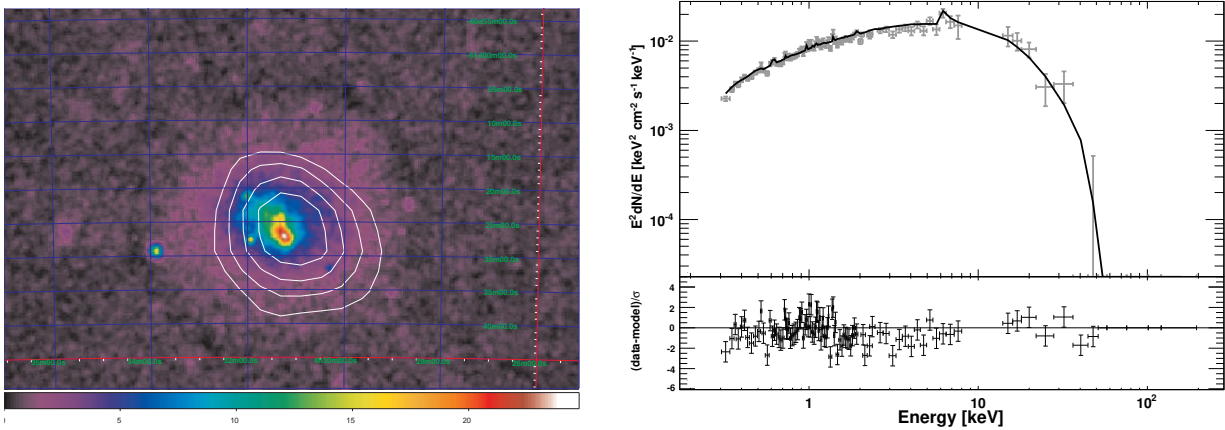


Fig. 4. Left Panel: ROSAT 0.1{2.4 keV surface brightness of Abell 3266 with BAT significance contours superimposed. The contours range from 2.5 to 5.5. Right Panel: Joint fit to XMM-Newton{BAT data for Abell 3266 with a thermal model. The best model is shown as solid line.

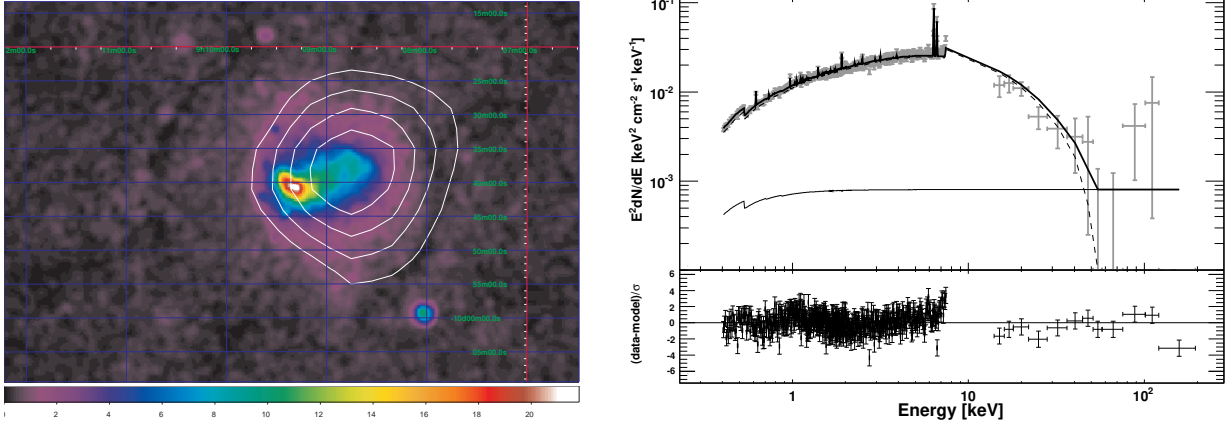


Fig. 5. Left Panel: ROSAT 0.1{2.4 keV surface brightness of Abell 0754 with BAT significance contours superimposed. The contours range from 2.5 to 8.0 . Right Panel: Joint fit to XMM-Newton/BAT data. The best fit model (thick solid line) is the sum of a thermal model (dashed line) and of a power law (thin solid line).

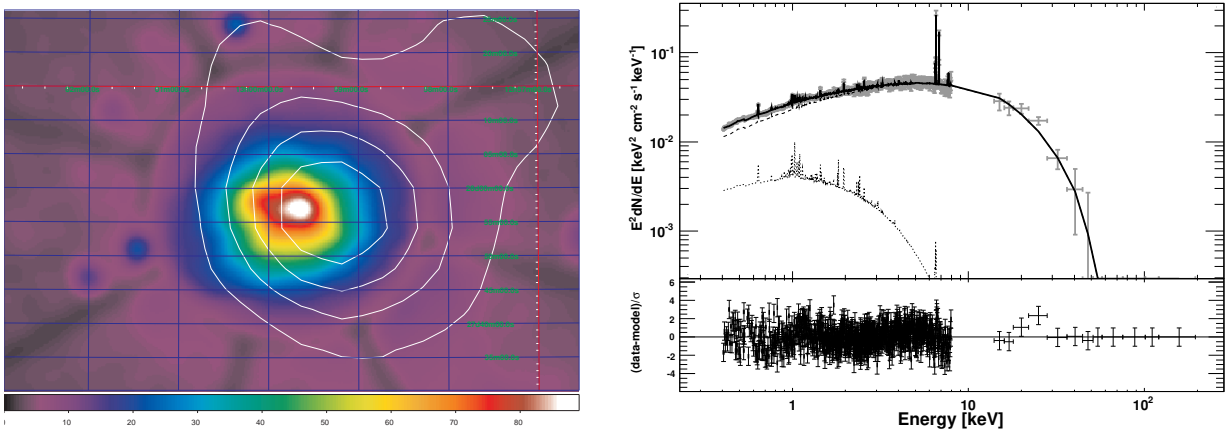


Fig. 6. Left Panel: ROSAT 0.1{2.4 keV surface brightness of Coma with BAT significance contours superimposed. The contours range from 2.5 to 20 . Right Panel: Joint fit to XMM-Newton/BAT data. The best fit model (solid line) is the sum of two thermal models (dashed and dotted lines).

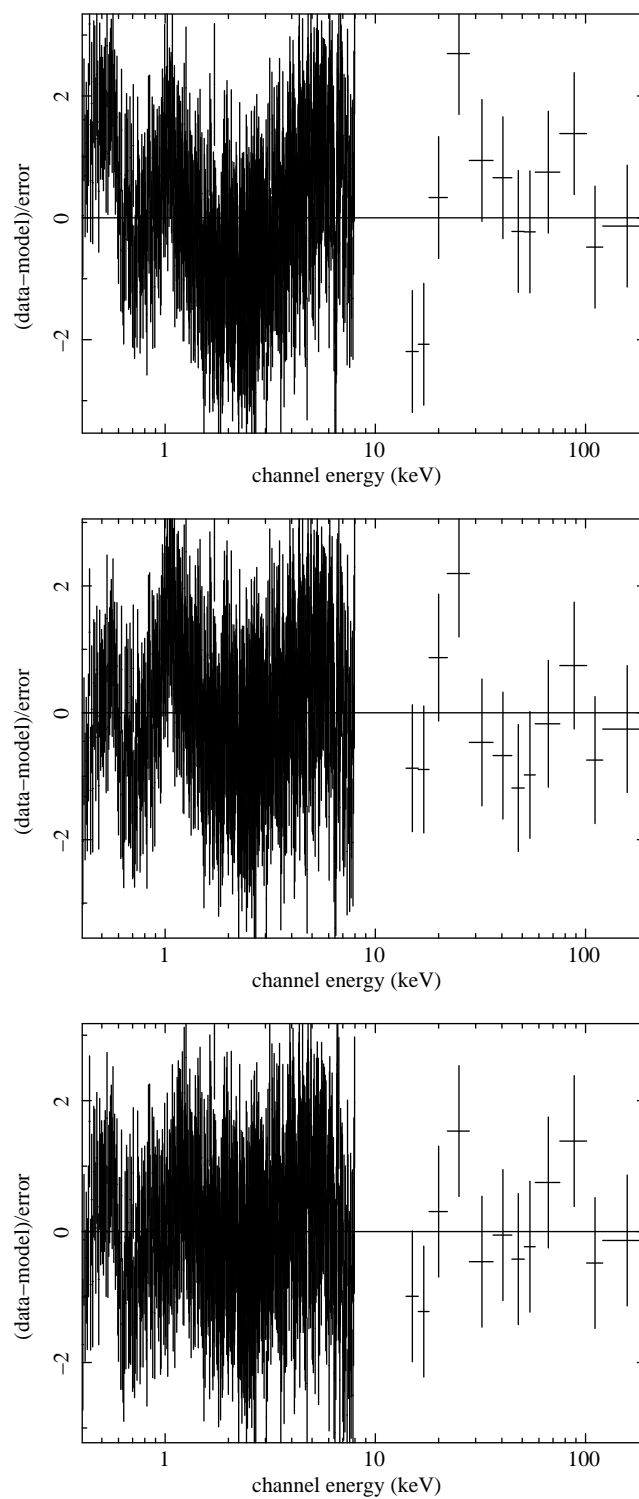


Fig. 7. Residuals to the fit to Coma data using: a single thermal model (top), sum of a thermal model and a power law (middle), and the sum of two thermal models (bottom).

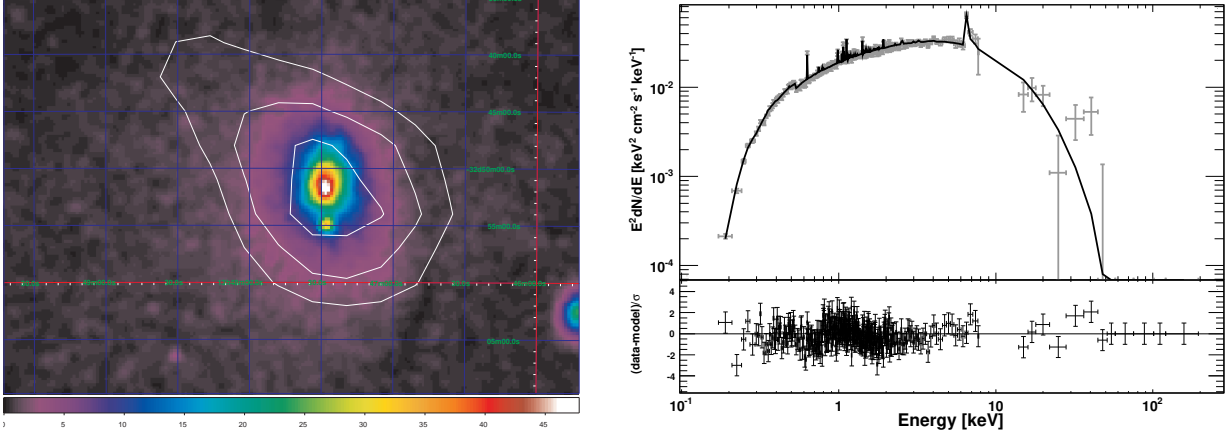


Fig. 8. Left Panel: ROSAT 0.1{2.4 keV surface brightness of Abell 3571 with BAT significance contours superimposed. The contours range from 2.5 to 5.0 . Right Panel: Joint fit to XMM-Newton/BAT data with a thermal model. The best fit model is shown as a solid line.

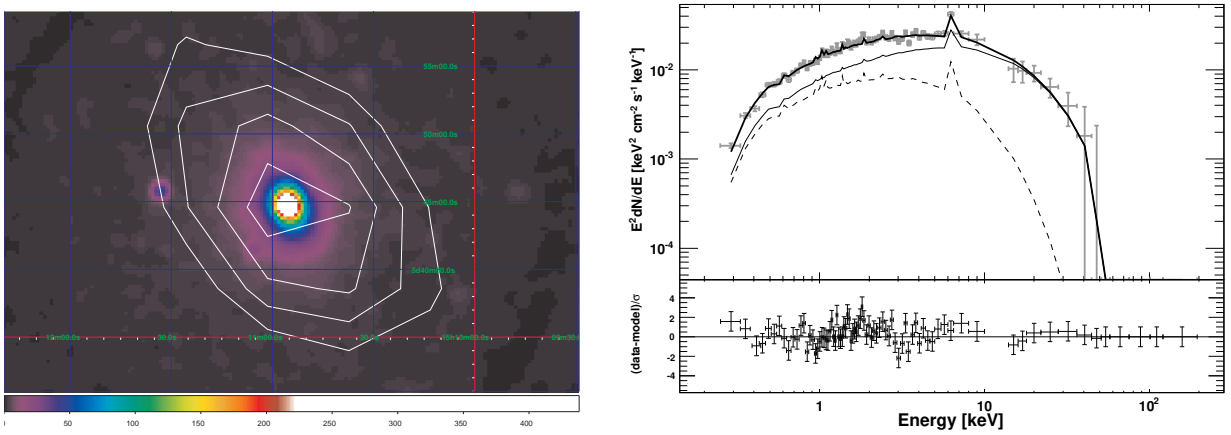


Fig. 9. Left Panel: ROSAT 0.1{2.4 keV surface brightness of Abell 2029 with BAT significance contours superimposed. The contours range from 2.5 to 5.0 . Right Panel: Joint XRT/BAT spectrum of Abell 2029. The best fit (thick solid line) is the sum of two thermal models (thin solid and dashed line).

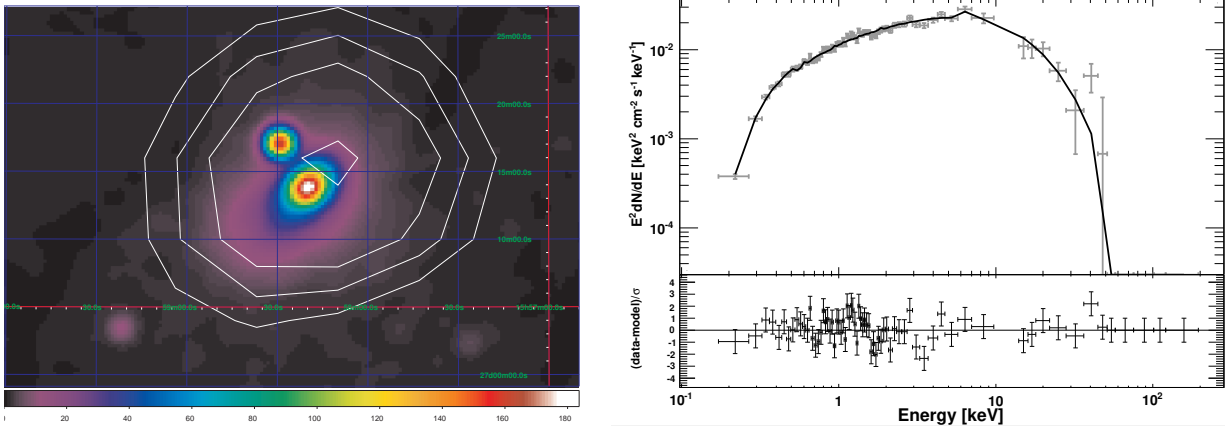


Fig. 10. | Left Panel: ROSAT 0.1{2.4 keV surface brightness of Abell 2142 with BAT significance contours superimposed. The contours range from 2.5 to 7.0 . Right Panel: Joint fit to XMM-Newton/BAT data for Abell 2142 with single thermal model. The best fit model is shown as a solid line.

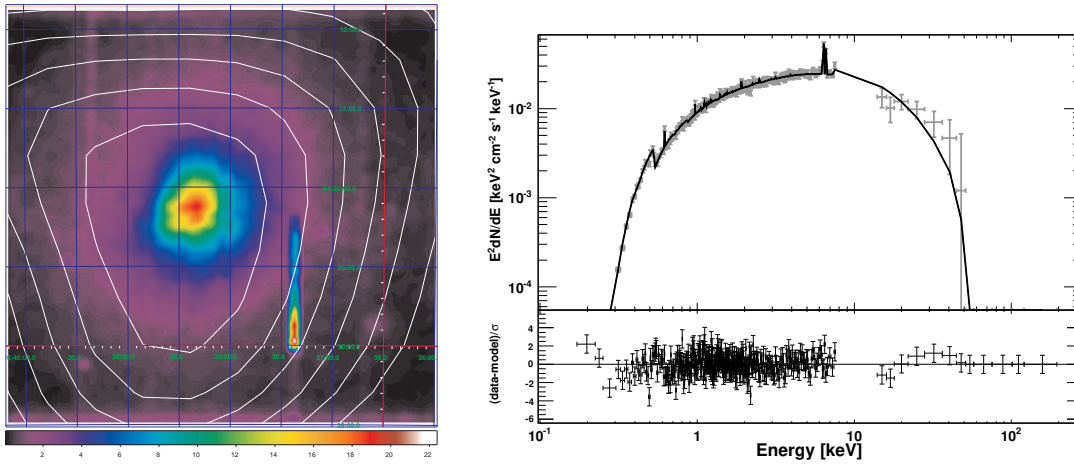


Fig. 11. | Left Panel: XMM-Newton 1.0{7.0 keV surface brightness of the Triangulum Australis cluster with BAT significance contours superimposed. The contours range from 2.5 to 7.0 . Right Panel: Joint fit to XMM-Newton/BAT data for the Triangulum Australis cluster with a thermal model. The best fit model is shown as a solid line.

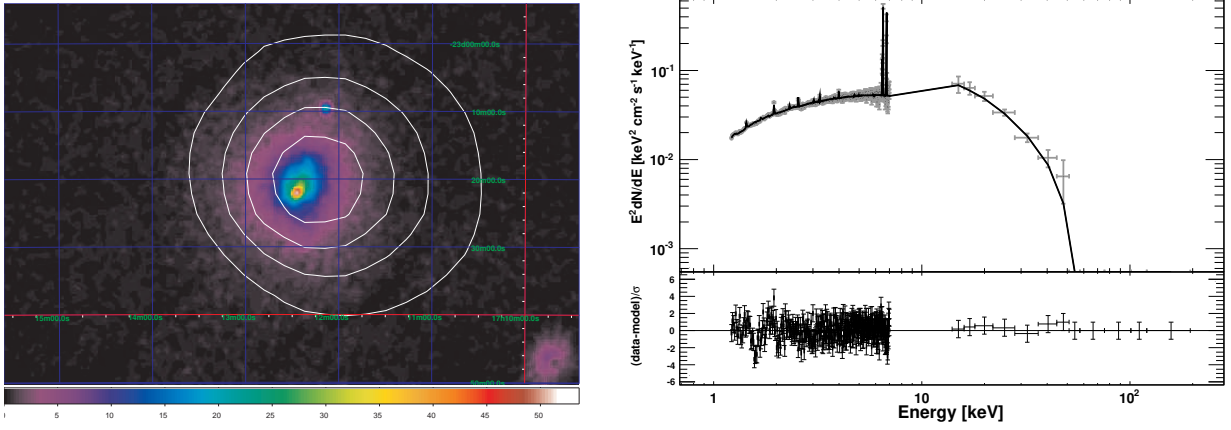


Fig. 12. Left Panel: ROSAT 0.1{2.4 keV surface brightness of the Ophiucus cluster with BAT significance contours superimposed. The contours range from 2.5 to 22 . Right Panel: Joint fit to Chandra/BAT data for the Ophiucus cluster with a thermal model. The best fit is shown as solid line.

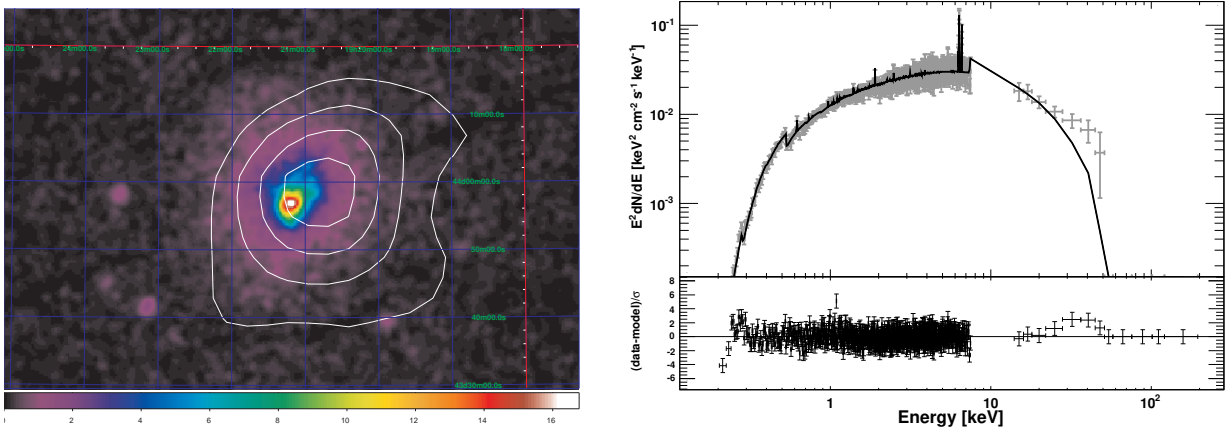


Fig. 13. Left Panel: ROSAT 0.1{2.4 keV surface brightness of Abell 2319 with BAT significance contours superimposed. The contours range from 2.5 to 22 . Right Panel: Joint fit to XMM-Newton/BAT data for Abell 2319 Australis cluster. The best fit model is shown as a solid line.

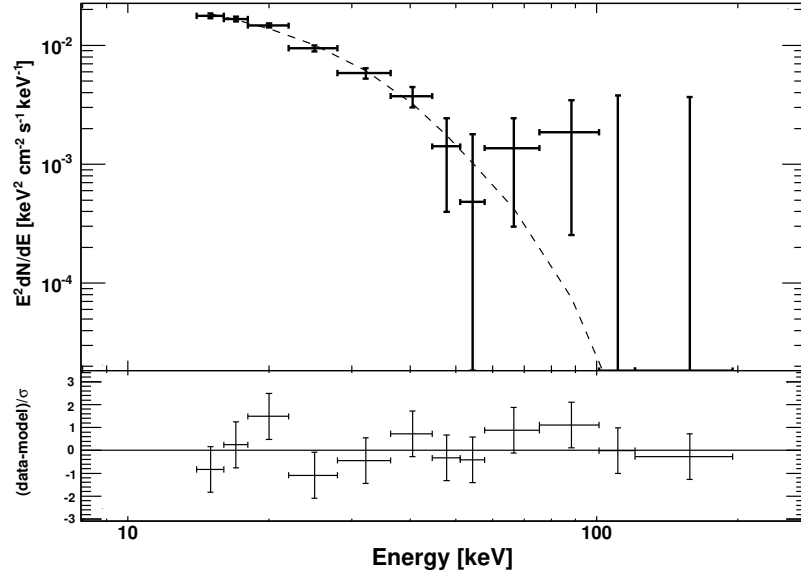


Fig. 14. | Stacked spectrum of the clusters in our sample and the best fit (dashed line) with a bremsstrahlung model.

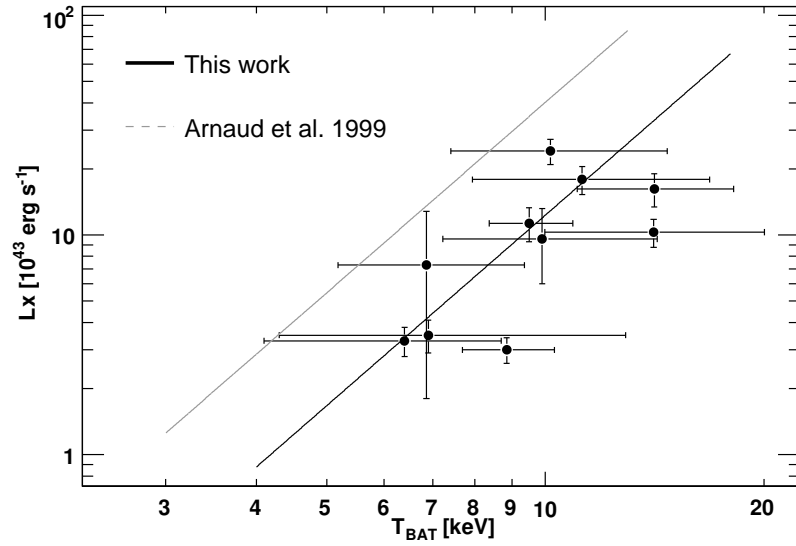


Fig. 15. | Luminosity-Temperature relation for the BAT clusters. The black line is the best, power-law, fit to the data while the gray line is the best fit of Arnaud & Evrard (1999) converted to the BAT energy band.

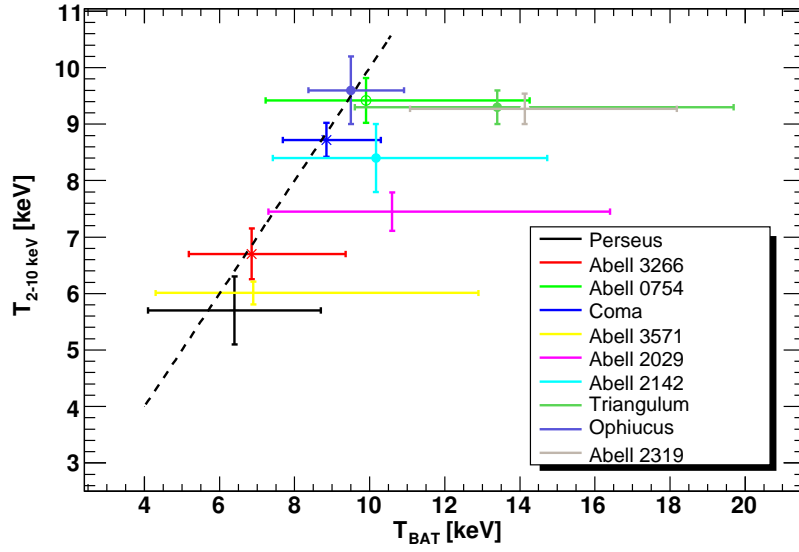


Fig. 16. Comparison of best fit gas temperatures. The x-axis reports the temperatures derived using BAT data (above 15 keV) while the y-axis shows the temperatures derived using 2-10 keV data (XMM-Newton, Chandra or XRT). The dashed line shows the $T_{\text{BAT}} = T_{2-10 \text{ keV}}$ function. The largest deviations are for the merging clusters Abell 2029 and Abell 2319.

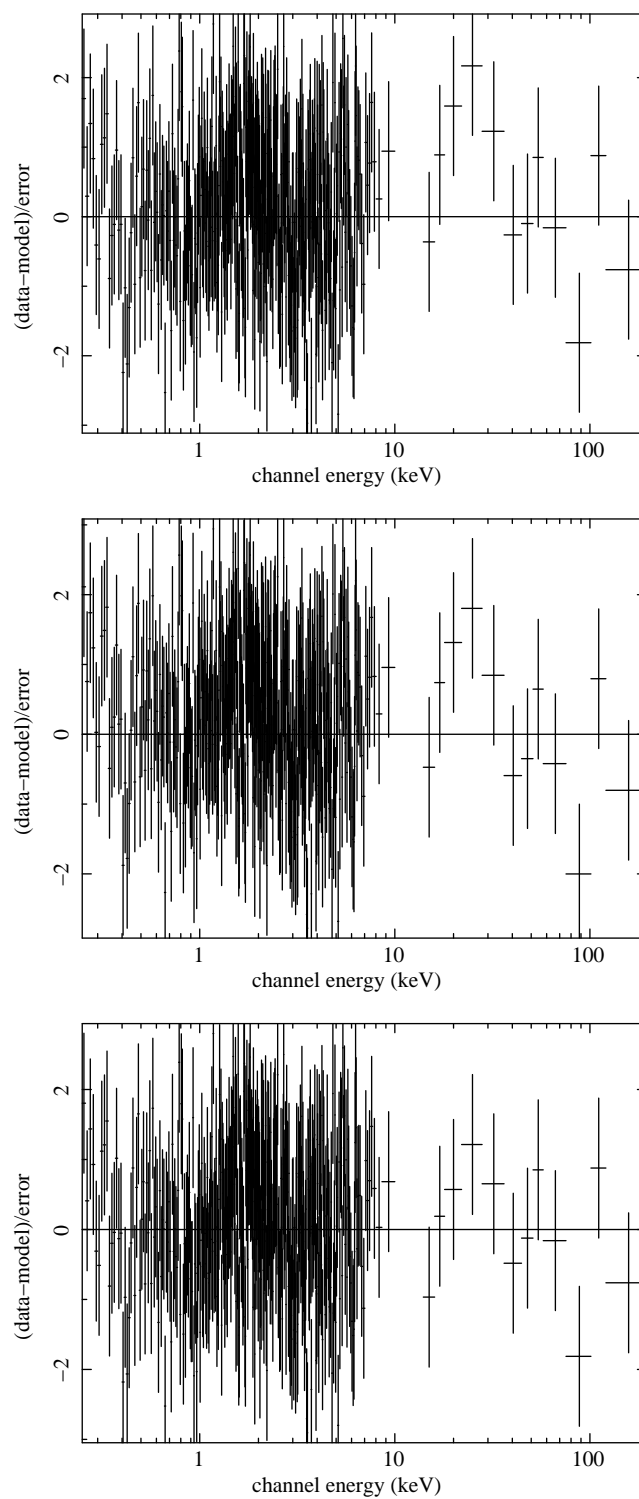


Fig. 17. Residuals to the fit to Abell 2029 data using: a single thermal model (top), sum of a thermal model and a power law (middle), and the sum of two thermal models (bottom).

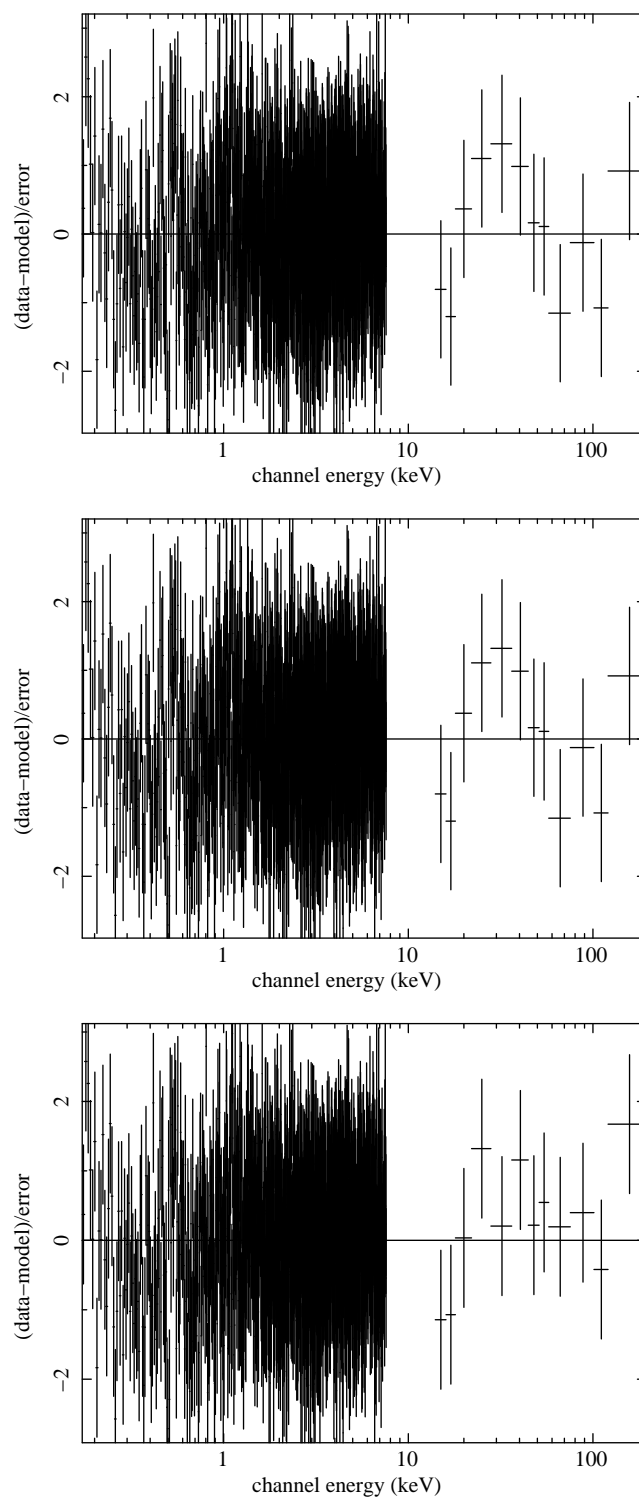


Fig. 18. Residuals to the fit to Triangulum Australis data using: a single thermal model (top), sum of a thermal model and a power law (middle), and the sum of two thermal models (bottom).

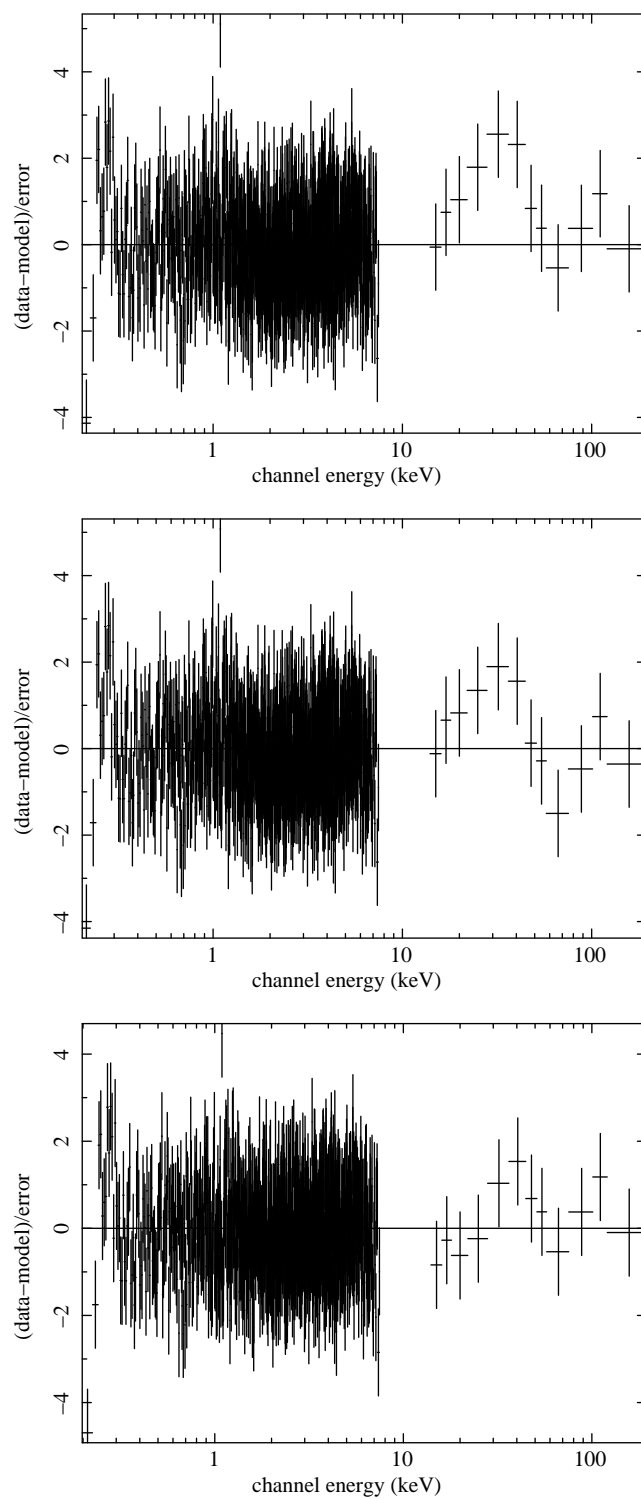


Fig. 19. Residuals to the fit to Abell 2319 data using: a single thermal model (top), sum of a thermal model and a power law (middle), and the sum of two thermal models (bottom).

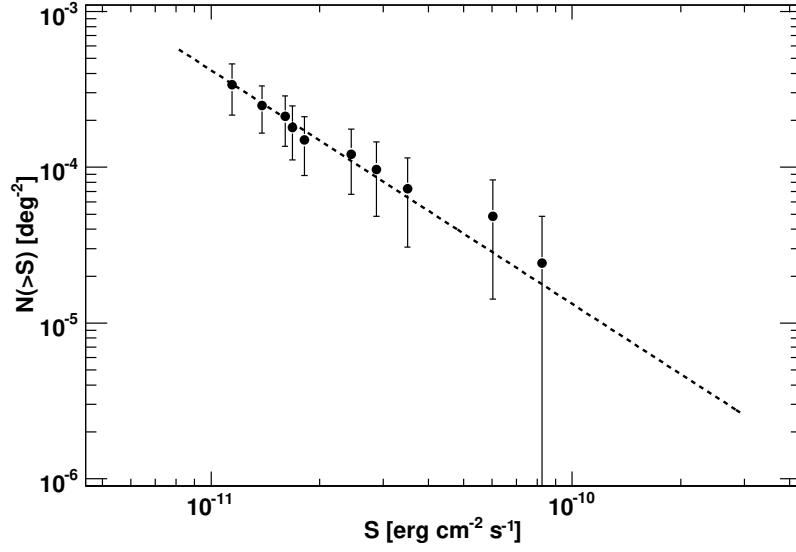


Fig. 20. Cumulative flux number relation for the BAT clusters (15{55 keV}). The dashed line is an overlaid power law $N(>S) = A S^{-1.5}$.

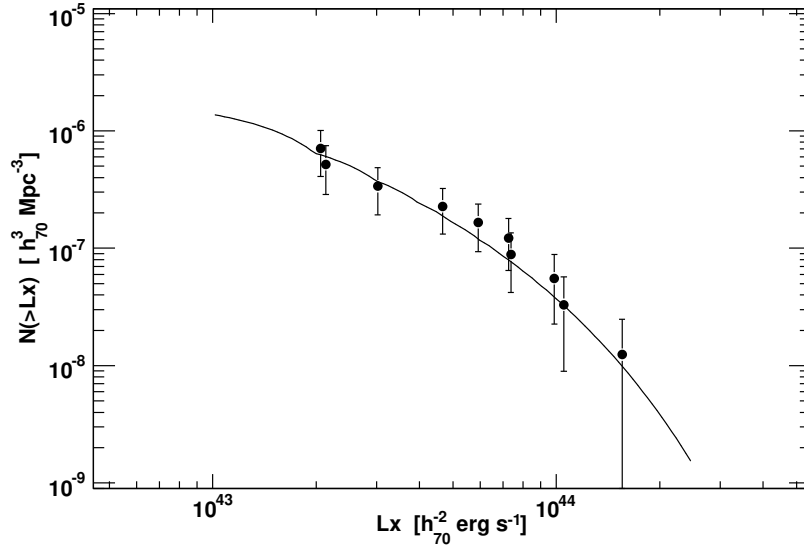


Fig. 21. Cumulative luminosity function of the BAT clusters (15{55 keV}). The solid line is the X-ray luminosity function determined for the REFLEX survey (Bohringer et al. 2002) converted to the BAT energy band.

Table 1. Clusters detected in the 15{55 keV band

NAME	R A .	DEC	S/N	ID	z	EXPOSURE	OFFSET
	(J2000)	(J2000)				(M s)	(arcmin)
J0319.8+ 4130	49.9573	41.5110	28.00	Perseus	0.0175	2.89	0.5
J0431.3-6126	67.8297	-61.4388	5.61	Abell 3266	0.0590	3.81	2.1
J0908.9-0938	137.2391	-9.6346	8.28	Abell 0754	0.0530	2.96	1.8
J1259.4+ 2757	194.8531	27.9523	19.95	Coma Cluster	0.0230	4.32	5.1
J1347.7-3253	206.9500	-32.9000	5.05	Abell 3571	0.0397	1.78	4.5
J1511.0+ 0544	227.7500	5.7485	5.33	Abell 2029	0.0770	2.71	0.8
J1558.5+ 2714	239.6256	27.2417	7.11	Abell 2142	0.0890	3.62	3.3
J1638.8-6424	249.7136	-64.4000	6.90	Triangulum A .	0.0510	1.77	4.9
J1712.3-2319	258.0914	-23.3242	21.63	Ophiucus	0.028	1.30	1.7
J1920.9+ 4357	290.2405	43.9646	11.72	Abell 2319	0.056	3.87	2.2

Table 2. Spectral parameters from combined XMM-Newton/XRT/Chandra and BAT fits
(errors are 90% C.L.)

NAME	Flux ^a (10 ⁻¹¹ cgs)	L _X ^a (10 ⁴³ erg s ⁻¹)	kT (keV)	model	χ^2/dof
Perseus	3.90 ^{+0.10} _{1.65}	2.7 ^{+0.1} _{1.1}	3.00 ^{+0.40} _{0.71} / 6.40 ^{+0.62} _{0.71}	1.7 ^{+0.3} _{0.7} apec+ apec+ pow	152.8/144
Abell 3266	0.73 ^{+0.10} _{0.11}	6.9 ^{+0.9} _{0.9}	8.0 ^{+0.4} _{0.4}	apec	666.8/841
Abell 0754	1.11 ^{+0.04} _{0.04}	8.3 ^{+0.3} _{0.3}	9.3 ^{+0.4} _{0.4}	apec+ pow	1217.0/1072
Coma ^b	2.33 ^{+0.23} _{0.22}	3.0 ^{+0.2} _{0.4}	8.40 ^{+0.25} _{0.24} / 1.45 ^{+0.21} _{0.11}	apec+ apec	846.5/856
Abell 3571	0.63 ^{+0.09} _{0.06}	2.7 ^{+0.3} _{0.4}	6.0 ^{+0.2} _{0.2}	apec	723.9/1367
Abell 2029	1.01 ^{+0.16} _{0.45}	16.8 ^{+2.4} _{4.7}	4.1 ^{+1.7} _{1.5} / 9.6 ^{+2.0} _{2.0}	apec+ apec	394.2/363
Abell 2142	0.90 ^{+0.10} _{0.10}	21.5 ^{+3.5} _{2.6}	8.40 ^{+0.64} _{0.45}	apec	361.9/398
Triangulum A.	1.30 ^{+0.10} _{0.10}	8.8 ^{+0.6} _{0.2}	9.30 ^{+0.30} _{0.30}	apec	925.8/1074
Ophiucus	5.7 ^{+0.5} _{0.5}	9.38 ^{+0.28} _{0.14}	9.93 ^{+0.24} _{0.24}	apec	323.1/351
Abell 2319	1.56 ^{+0.14} _{0.14}	13.0 ^{+0.9} _{0.8}	9.23 ^{+0.27} _{0.27}	apec	1151.3/1274

^aFlux and Luminosities are computed in the 15–55 keV band.

^bThe spectral values reported for Coma are only representative for the source extraction region (i.e. 10⁰ around the BAT centroid; see x 2.4.4 for more details).

Table 3. 3 Upper limits on the non-thermal component and Clusters' properties

NAME	CC ^a ?	Merger ?	$F_{50-100\text{ keV}}^b$ ($10^{-12}\text{ erg cm}^{-2}\text{ s}^{-1}$)	B (G)	S_{radio} (Jy)	ν_{radio} (MHz)	Ref ^c
Perseus	y	y					
Abell 3266	n	y	< 5.30	> 0.17	1.070	2700	0.95 1
Abell 0754	n	y	< 6.50	> 0.10	0.086	1365	1.5 2
Coma	n	y					
Abell 3571	y ^d	n ^e	< 11.5	> 0.03	0.0084	1380	1.5 ^g 3
Abell 2029	y ^d	y	< 4.83	> 0.25	0.528	1380	1.5 ^g 4
Abell 2142	y ^f	y	< 5.35	> 0.06	0.0183	1400	1.5 ^g 5
Triangulum A.	y ^f	y ^f	< 4.65	> 0.17	< 0.033	4850	1.5 ^g 6
Ophiucus	n	n	< 5.89	> 0.11	6.4	160	2.0 7
Abell 2319	y ^d	y	< 3.41	> 0.10	1.0	610	0.92 8

^aCC = Cool Core^bBAT data alone were used to estimate the upper limits^cReferences for the radio flux^dModerate CC^eThe morphology and temperature map indicate that it is a relaxed cluster, but the radio structure points at late stages of merging^fUnder discussion^gArbitrary spectral index

References. | 1) Brown & Burns (1991), 2) Fusco-Femiano et al. (2003), 3) Condon et al. (1998), 4) Giovannini & Feretti (2000), 5) Condon et al. (1993), 6) Slee (1977), 7) Feretti et al. (1997).

Table 4. Non-thermal emission from combined XMM-Newton/XRT/Chandra and BAT data.

NAME	$F_{50-100\text{keV}}^a$ ($10^{-12}\text{erg cm}^{-2}\text{s}^{-1}$)	B^b (G)
Perseus		
Abell 3266	< 0.57	> 0.55
Abell 0754		
Coma		
Abell 3571	$1.4^{+0.4}_{-0.4}$	0.08
Abell 2029	< 1.27	> 0.42
Abell 2142	< 1.50	> 0.10
Triangulum Australis	< 0.65	> 0.39
Ophiucus	< 2.80	> 0.15
Abell 2319	< 0.67	> 0.15

^aThe flux has been estimated using a power-law spectrum with a photon index of 2.0 in the 10-200 keV energy band. Upper limits are 99% CL while errors are 90% CL.

^bIn order to compute the intensity of the magnetic field we used the same Radio data reported in Tab. 3

Table 5: Comparison of different spectral fits to the clusters which show a large deviation between the ICM temperature as measured below and above 10 keV. As a reference for the reader also the parameters of Coma are reported. kT_1 and kT_2 are the temperatures of the two thermal models (in keV) while norm. and Γ are the normalization at 1 keV (in $\text{ph cm}^{-2} \text{s}^{-1} \text{keV}^{-1}$) and the photon index of the power-law model. Frozen parameters do not have an error estimate.

Cluster	Thermal	Thermal+ power law	Thermal+ Thermal
Abell 2029			
kT_1	$6.75^{+0.52}_{-0.31}$	$6.78^{+0.46}_{-0.33}$	$4.1^{+1.7}_{-1.5}$
norm.		2.0	
kT_2		$1.55^{+1.12}_{-1.15} 10^3$	$9.6^{+2.0}_{-2.0}$
χ^2/dof	407.3/364	402.1/363	394.2/363
Triangulum A.			
kT_1	$9.30^{+0.30}_{-0.30}$	$9.25^{+0.30}_{-0.28}$	$11.1^{+0.34}_{-0.27}$
norm.		2.0	
kT_2		$< 1.40 10^4$	$1.63^{+0.46}_{-0.27}$
χ^2/dof	925.8/1074	925.8/1073	916.5/1072
Abell 2319			
kT_1	$9.23^{+0.27}_{-0.27}$	$9.33^{+0.35}_{-0.52}$	$11.2^{+0.8}_{-1.0}$
norm.		$1.7^{+0.2}_{-0.3}$	
kT_2		$7.8^{+2.7}_{-5.3} 10^4$	$1.9^{+1.64}_{-0.40}$
χ^2/dof	1151.34/1274	1139.9/1272	1127.8/1272
Coma			
kT_1	$6.50^{+0.09}_{-0.05}$	$7.19^{+0.16}_{-0.06}$	$8.40^{+0.25}_{-0.24}$
norm		$2.11^{+0.10}_{-0.13}$	
kT_2		$3.56^{+0.46}_{-0.34} 10^3$	$1.45^{+0.21}_{-0.11}$
χ^2/dof	1168.9/858	905.5/856	846.5/856